Annu. Rev. Nucl. Part. Sci. 2000. 50:525–75

PROSPECTS FOR SPIN PHYSICS AT RHIC

Gerry Bunce,[1] Naohito Saito,[2] Jacques Soffer,[3] and Werner Vogelsang[4]

[1]*Brookhaven National Laboratory, Upton, New York 11973-5000 and RIKEN BNL Research Center, Brookhaven National Laboratory, Upton, New York 11973-5000; e-mail: bunce@bnl.gov*

[2]*RIKEN (The Institute of Physical and Chemical Research), Wako, Saitama 351-0198, Japan, and RIKEN BNL Research Center, Brookhaven National Laboratory, Upton, New York 11973-5000; e-mail: saito@bnl.gov*

[3]*Centre de Physique Théorique–CNRS–Luminy, Case 907, F-13288 Marseille Cedex 9, France; e-mail: Jacques.Soffer@cpt.univ-mrs.fr*

[4]*C.N. Yang Institute for Theoretical Physics, State University of New York at Stony Brook, Stony Brook, New York 11794-3840 and RIKEN BNL Research Center, Brookhaven National Laboratory, Upton, New York 11973-5000; e-mail: wvogelsang@bnl.gov*

Key Words proton spin structure, spin asymmetries, quantum chromodynamics, beyond the standard model

■ **Abstract** Colliding beams of 70% polarized protons at up to $\sqrt{s} = 500\,\text{GeV}$, with high luminosity, $\text{L} = 2 \times 10^{32}\,\text{cm}^{-2}\,\text{sec}^{-1}$, will represent a new and unique laboratory for studying the proton. RHIC-Spin will be the first polarized-proton collider and will be capable of copious production of jets, directly produced photons, and W and Z bosons. Features will include direct and precise measurements of the polarization of the gluons and of $\overline{u}$, $\overline{d}$, u, and d quarks in a polarized proton. Parity violation searches for physics beyond the standard model will be competitive with unpolarized searches at the Fermilab Tevatron. Transverse spin will explore transversity for the first time, as well as quark-gluon correlations in the proton. Spin dependence of the total cross section and in the Coulomb nuclear interference region will be measured at collider energies for the first time. These qualitatively new measurements can be expected to deepen our understanding of the structure of matter and of the strong interaction.

CONTENTS

1. INTRODUCTION

Spin is a powerful and elegant tool in physics. One of the most exciting aspects of physics is a search for the unexpected, the nonintuitive, in nature. Intrinsic spin itself violates our intuition, in that an elementary particle such as an electron can both be pointlike and have a perpetual angular momentum. We find at this time an apparent violation of our intuition in the proton. We understand the proton as being composed of quarks, gluons, and antiquarks, and we expect the proton spin to be carried dominantly by its three valence quarks. Instead, through the 1980s and 1990s, deep inelastic scattering (DIS) experiments of polarized electrons and muons from polarized nucleons have shown that on average only about 1/4 to 1/3 of the proton spin is carried by the quarks and antiquarks in the proton (1). Therefore, the spin of the proton appears to be mainly carried by the gluons and orbital angular momentum! This surprising and counterintuitive result indicates that the proton, and particularly its spin structure, is much more interesting than we had thought.

Spin can be used as an elegant tool to search for the unexpected. If an experiment is found to depend on the spin direction, it can violate a deep expectation that physics should be symmetric with respect to that axis. An example is mirror symmetry, i.e. that physics should not depend on left- or right-handedness. The violation of parity by the weak interaction was the surprise that led to the present electroweak model with the purely left-handed charged weak vector bosons $W^{\pm}$. At the Relativistic Heavy Ion Collider (RHIC) at Brookhaven National Laboratory, the W^+ and W^- will be produced by colliding beams of protons spinning alternately left- and right-handed. The expected maximum violation of parity will allow unique and precise measurements of the spin direction of the quarks and antiquarks in the proton that form the W bosons, identified by quark flavor, u, $\overline{u}$, d, and $\overline{d}$. A dependence on handedness in the production of jets at RHIC beyond

the contribution from W and Z would directly signal new physics, possibly coming from quark substructure at a scale above the weak scale.

Physics is also a search for unexpected order in nature. Large spin effects necessarily imply coherence and order. If the gluons in a proton are found to be dominantly spinning in the same direction, as discussed widely in the context of the smallness of the quark spin contribution (reviewed in Reference 2), there would need to be a simple underlying physical mechanism that creates this order. At RHIC, dedicated experiments will measure the direction of the gluon spin in the proton for the first time—an exciting prospect, since there are hints that the gluon polarization may be substantial.

The RHIC at Brookhaven began a program of colliding beams of gold ions at 100 GeV per nucleon in the spring of 2000. The following year, the first physics run colliding beams of polarized protons is expected. RHIC-Spin will be the first polarized proton-proton collider. It will reach an energy and luminosity at which the collisions can clearly be interpreted as collisions of polarized quarks and gluons, and it will be capable of copious production of jets and directly produced photons, as well as W and Z bosons. Quantum chromodynamics (QCD) makes definite predictions for the hard spin interactions of quarks and gluons, which implies that RHIC will enable us to test a sector of QCD that so far has been little explored. The polarized quark and gluon probes at RHIC complement the beautiful work done using polarized lepton probes to study proton spin structure. These strong interaction probes will be sensitive to the gluon polarization in jet and direct photon production and will allow quark spin-flavor separation in $W^{\pm}$ production. RHIC-Spin will also represent the highest energy for proton-proton collisions at accelerators, and unpolarized $W^{\pm}$ production will be used to precisely measure the flavor asymmetry of the antiquark sea.

At the Polarized Collider Workshop at Penn State University in 1990 (3), the exploration of the spin of the proton was a major focus for the physics of polarized proton collisions at RHIC. The RHIC-Spin Collaboration was formed the following year, consisting of experimenters, theorists, and accelerator physicists (4). Since 1993, the two large heavy ion detectors at RHIC, STAR and PHENIX, have considered spin as a major program and include additional apparatus specifically for spin physics. In addition, the PP2PP experiment at RHIC, studying small-angle elastic scattering, will also feature spin. The present article presents the anticipated physics of the RHIC spin program as developed by the RHIC-Spin Collaboration and by the STAR, PHENIX, and PP2PP Collaborations.

The RHIC spin accelerator complex is illustrated in Figure 1. An intense polarized H^- source feeds a chain of accelerators. Individual bunches of 2×10^{11} protons with 70% polarization are transferred from the Alternating Gradient Synchrotron (AGS) to the RHIC rings at 22 GeV. This is repeated 120 times for each ring at RHIC. The polarized protons are then accelerated to up to 250 GeV in each ring for collisions at each of six intersection regions. With a $\beta^* = 1$ m focus at STAR and PHENIX, luminosity will be $\mathcal{L} = 2 \times 10^{32}$ cm^{-2} s^{-1}, for the highest RHIC energy of $\sqrt{s} = 500$ GeV. Experimental sensitivities given in this article

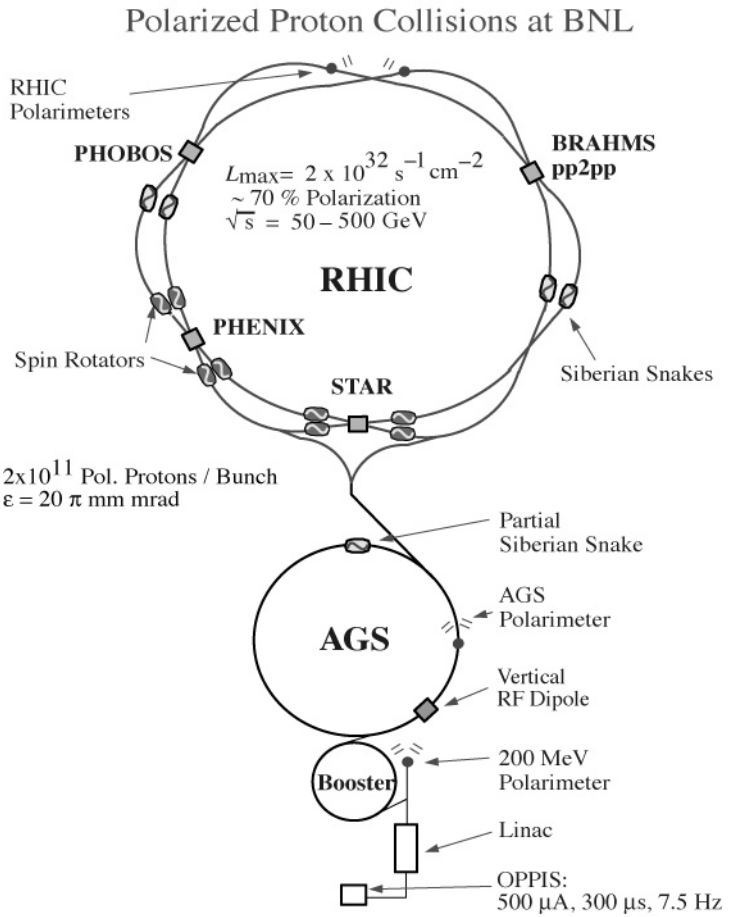

Figure 1 Schematic layout of the RHIC accelerator complex. Only relevant devices for polarized *pp* collisions are shown.

are based on 800 pb^{-1} for $\sqrt{s} = 500$ GeV and 320 pb^{-1} for $\sqrt{s} = 200$ GeV. This corresponds to runs of 4×10^6 s at full luminosity, about four months of running with 40% efficiency, at each energy. We expect the data to be collected over three to four years, since RHIC is shared between heavy-ion and polarized-proton collisions. The expected sensitivities will be excellent due to the high luminosity for proton-proton collisions. For comparison, we note that the $\overline{p}p$ Tevatron at Fermilab has run for a total of ∼130 pb^{-1} as of 1999.

It is difficult to maintain the proton polarization through acceleration because of its large anomalous magnetic moment: The proton spin readily responds to focusing and error magnetic fields in the rings, and spin resonances are encountered

frequently, for example at every 500 MeV of acceleration in the AGS. The methods that are used to avoid depolarization in acceleration are very elegant, and the acceleration of polarized protons to 250 GeV will be breaking new ground in accelerator physics. The key device is a string of dipole magnets that rotate the proton spin 180° around a selected axis in the horizontal plane each time the beam passes (5). Each two passes in effect cancel the cumulative tilt of the spin resulting from horizontal magnetic fields, thus eliminating the major spin resonances at RHIC. There will be four "Siberian Snakes" at RHIC, two in each ring. The name refers to the home institution of the inventors (Novosibirsk) and to the motion of the beam passing through. In this article, we do not discuss the accelerator physics work leading to the RHIC spin plan (6), but, as for any spin experiment, past or future, there is a very tight, necessary, and refreshing coupling between the polarization technology and the physics.

For two Siberian Snakes in each ring, the stable spin direction in RHIC will be vertical. Therefore, transverse spin physics will be available to all the experiments. For STAR and PHENIX, special strings of dipole magnets will be used to rotate the spin to longitudinal at their intersection regions. Longitudinal spin is necessary to study gluon polarization and parity-violating physics. A recent plan (7) is to initially use one Siberian Snake in each ring, which allows the construction and installation of the Snakes and Rotators to be staged. With a single Snake in a ring, the stable spin direction is in the horizontal plane. If the beam is inserted into RHIC, and the Snake is then turned on adiabatically, the spin will follow from vertical to horizontal. At energies roughly 2 GeV apart, it will be possible to have longitudinal polarization at all six intersection regions, up to a beam energy of 100 GeV. One Snake is already installed in RHIC at this time, and a second Snake will be completed in summer 2000. Therefore, the RHIC-Spin program will be ready for its commissioning in summer 2000 and ready for the first spin physics run with longitudinal polarization at $\sqrt{s} = 200$ GeV in 2001.

2. PREREQUISITES FOR SPIN PHYSICS AT RHIC

2.1 Theoretical Concepts and Tools

2.1.1 Partons in High-Energy Scattering: Factorization Polarized pp collisions at RHIC will take place at center-of-mass energies of $\sqrt{s} = 200$–500 GeV. Except for polarization, we have a typical collider physics situation, similar to that at CERN's Sp$\overline{\text{p}}$S or the Tevatron at Fermilab. One therefore expects that parton model concepts, augmented by the predictive power of perturbative QCD, will play a crucial role in describing much of the interesting spin physics to be studied at RHIC, if the reaction under consideration involves a hard probe, for instance a photon produced at transverse momentum (p_T) of a few GeV or more.

The QCD-improved parton model has been successfully applied to many high-energy processes involving hadrons in the initial or final state. In this framework,

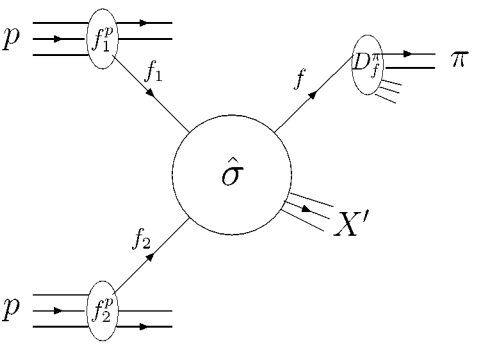

Figure 2 Production of a large-p_T pion in a hard pp collision.

a cross section is written in a factorized form as a convolution of appropriate parton densities and/or fragmentation functions with a partonic subprocess cross section. The predictive power of perturbative QCD follows from the universality of the distribution functions: Once extracted from the data in one process, they can be used to make definite predictions for any other. As an example, let us consider the production of a pion with large p_T in a collision of unpolarized protons, that is, $pp \to \pi X$. The process is depicted in Figure 2. In the parton model framework, in the context of QCD perturbation theory, one writes the cross section as a convolution,

$$\frac{d\sigma^{pp\to\pi X}}{d\mathcal{P}} = \sum_{f_1, f_2, f} \int dx_1 dx_2 dz f_1^p(x_1, \mu^2)\, f_2^p(x_2, \mu^2) \times \frac{d\hat{\sigma}^{f_1 f_2 \to f X'}}{d\mathcal{P}}(x_1\, p_1, x_2\, p_2, p_\pi/z, \mu) D_f^\pi(z, \mu^2), \qquad 1.$$

where p_1 and p_2 are the incident proton momenta. Here, $\mathcal{P}$ stands for any appropriate set of the kinematic variables of the reaction. Furthermore, $f_i^p(x, \mu^2)$ is introduced as the probability density for finding a parton of type f_i in the proton, which has taken fraction x of the proton's momentum. Likewise, $D_f^\pi(z, \mu^2)$ is the probability density for finding a pion with momentum fraction z in the parton f. The $\hat{\sigma}^{f_1 f_2 \to f X'}$ are the underlying hard-scattering cross sections for initial partons f_1 and f_2 producing a final-state parton f plus unobserved X'.

The functions f^p and D_f^π introduced in Equation 1 express intrinsic properties of the proton and of the hadronization mechanism, respectively. Therefore, they are sensitive to non-perturbative physics and cannot be calculated from first principles in QCD at present. In contrast to this, for a sufficiently hard process, it will make sense to calculate the subprocess cross sections $\hat{\sigma}^{f_1 f_2 \to f X'}$ as perturbation series in the strong coupling α_s. The separation of short-distance and long-distance phenomena as embodied in Equation 1 necessarily implies the introduction of an unphysical mass scale μ, the factorization scale. The presence of μ arises in practice when computing higher-order corrections to the $\hat{\sigma}^{f_1 f_2 \to f X'}$.

Here, one encounters singularities resulting from configurations in which one of the incoming (massless) partons collinearly emits another parton. In the same way, such "collinear" singularities (or "mass" singularities) occur in the final state from collinear processes involving parton f. Regularization of the mass singularities always introduces an extra mass scale M to the problem; the cross section depends on it through powers of "large" logarithms of the type $\ln(p_T/M)$. The collinear-singular logarithms are separated off at the factorization scale μ, to be of the order of the hard scale p_T characterizing the hard interaction, and are absorbed ("factorized") into the "bare" parton densities (or fragmentation functions). This procedure is of use only if it is universal in the sense that the mass singularities absorbed into the parton densities are the same for all processes involving a given initial parton. Proof of this property is the subject of factorization theorems (8, 9) and is necessary for the parton model to be valid in the presence of QCD interactions.

In summary, the QCD-improved parton-model picture as used for Equation 1 consists of perturbatively calculable partonic hard-scattering cross sections and of scale-dependent parton densities and fragmentation functions that are universal in the sense that once they are measured in one process, they can be used to make predictions for any other hard process. It is important to point out that the parton densities and fragmentation functions are never entirely nonperturbative: Their dependence on the factorization scale is calculable perturbatively, once the densities are known at some initial scale μ_0. This has to be so, since the μ-dependence of the $\hat{\sigma}^{f_1 f_2 \to f X'}$ is calculable and the prediction of a physical quantity, such as the hadronic cross section $\sigma^{pp\to\pi X}$, has to be independent of μ to the order of perturbation theory considered. The tool to calculate the dependence of the f^p and D_f^π on the "resolution scale" μ is the set of evolution equations (10).

2.1.2 Spin-Dependent Parton Densities and Cross Sections So far we have disregarded the *spin* information contained in parton distributions and fragmentation functions. If a hard-scattering process with incoming protons having definite spin orientation is studied, as at RHIC, one expects it to give information on the spin distributions of quarks and gluons in a polarized proton. The possible parton distribution functions (11) are summarized in Table 1. A similar table could be presented for polarized fragmentation functions (12): The observation of the polarization of a final-state hadron should give information on the polarization of the parton fragmenting into that hadron.

Within roughly the past decade, beautiful data (1) have become available that are sensitive to the "longitudinally" polarized ("helicity-weighted") parton densities of the nucleon. The tool to obtain such information has been deep-inelastic scattering (DIS) of longitudinally polarized leptons and nucleons. The spin asymmetry measured in such reactions gives information on the probability of finding a certain parton type ($f = u, \overline{u}, d, \overline{d}, \ldots, g$) with positive helicity in a nucleon of positive helicity, minus the probability for finding it with negative helicity (see Table 1). These densities are denoted as $\Delta f(x, \mu^2)$. The Appendix provides a brief discussion of the implications of present polarized DIS data on our knowledge

TABLE 1 Compilation of quark and gluon parton densities including spin dependence[a]

Polarization	Quarks	Gluons
Unpolarized	$q \equiv q_+^+ + q_+^- \equiv q_\uparrow^\uparrow + q_\uparrow^\downarrow$	$g \equiv g_+^+ + g_+^-$
Long, polarized	$\Delta q = q_+^+ - q_+^-$	$\Delta g = g_+^+ - g_+^-$
Transversity	$\delta q = q_\uparrow^\uparrow - q_\uparrow^\downarrow$	—

[a]The ubiquitous argument (x, μ^2) of the densities has been suppressed. For brevity, a column for antiquarks $(\overline{q})$ was omitted, which would have an identical structure to that of the quark column. Labels $+, -$ denote helicities, and $\uparrow, \downarrow$ transverse polarizations. Superscripts refer to partons and subscripts to the parent hadron.

about the Δf. Within a parton-model concept, the integrals of the $\Delta f(x, \mu^2)$ over all momentum Bjorken-x ("first moments"), multiplied by the spin of the parton f, will by definition give the amount of the proton's spin carried by species f, appearing in the proton-spin sum rule:

$$\frac{1}{2} = \int_0^1 dx \left[\frac{1}{2} \sum_q (\Delta q + \Delta \overline{q})(x, \mu^2) \; + \; \Delta g(x, \mu^2) \right] \; + \; L(\mu^2), \qquad 2.$$

where L is the orbital angular momentum of quarks and gluons in the proton (13).

The longitudinally polarized parton distributions in Table 1 can be separated from the unpolarized ones if suitable differences of cross sections for various longitudinal spin settings of the initial hadrons are taken (14):

$$\begin{aligned} \frac{d\Delta\sigma^{pp\to\pi X}}{d\mathcal{P}} &\equiv \frac{1}{4}\left[\frac{d\sigma_{++}^{pp\to\pi X}}{d\mathcal{P}} - \frac{d\sigma_{+-}^{pp\to\pi X}}{d\mathcal{P}} - \frac{d\sigma_{-+}^{pp\to\pi X}}{d\mathcal{P}} + \frac{d\sigma_{--}^{pp\to\pi X}}{d\mathcal{P}} \right] \\ &= \sum_{f_1, f_2, f} \int dx_1 dx_2 dz \; \Delta f_1^p(x_1, \mu^2) \; \Delta f_2^p(x_2, \mu^2) \\ &\quad \times \frac{d\Delta\hat{\sigma}^{f_1 f_2 \to f X'}}{d\mathcal{P}}(x_1, p_1, x_2, p_2, p_\pi/z, \mu) \; D_f^\pi(z, \mu^2), \qquad 3. \end{aligned}$$

where

$$\frac{d\Delta\hat{\sigma}^{f_1 f_2 \to f X'}}{d\mathcal{P}} \equiv \frac{1}{4}\left[\frac{d\hat{\sigma}_{++}^{f_1 f_2 \to f X'}}{d\mathcal{P}} - \frac{d\hat{\sigma}_{+-}^{f_1 f_2 \to f X'}}{d\mathcal{P}} - \frac{d\hat{\sigma}_{-+}^{f_1 f_2 \to f X'}}{d\mathcal{P}} + \frac{d\hat{\sigma}_{--}^{f_1 f_2 \to f X'}}{d\mathcal{P}} \right]. \qquad 4.$$

Here and in Equation 3, subscripts denote the helicities of the incoming particles, i.e. of the protons in Equation 3 and of partons f_1, f_2 in Equation 4. Thus, the "longitudinally polarized" cross section $d\Delta\sigma^{pp\to\pi X}/d\mathcal{P}$ depends only[1] on the

[1]In addition, there is dependence on the pion fragmentation functions D_f^π.

parton densities for longitudinal polarization and on the (calculable) "longitudinally polarized" subprocess cross sections $d\Delta\hat{\sigma}^{f_1 f_2 \to f X'}/d\mathcal{P}$. A measurement of $d\Delta\sigma^{pp\to\pi X}/d\mathcal{P}$ therefore gives access to the Δf. Adding, on the other hand, all terms in the first line of Equation 3, one simply returns to the unpolarized cross section in Equation 1, with its unpolarized densities f and the unpolarized subprocess cross sections $d\hat{\sigma}^{f_1 f_2 \to f X'}/d\mathcal{P}$, corresponding also to taking the sum of the terms in Equation 4.

Notice that we have taken both initial protons to be polarized in Equation 3. If only one is polarized, we can still define a singly polarized cross section by $d\sigma_-^{pp\to\pi X}/d\mathcal{P} - d\sigma_+^{pp\to\pi X}/d\mathcal{P}$, where the subscript refers to the polarized proton's helicity. However, this combination can be nonzero only if parity is violated in the hard process (14). If so, the single-spin cross section will depend on products of parton densities Δf_1 and f_2, representing the polarized and the unpolarized proton, respectively.

With two transversely polarized beams, one will take the first line of Equation 3 for transverse polarizations rather than helicities. The result will be a polarized cross section depending on transversely polarized subprocess cross sections and, for each proton, on the differences of distributions of quarks (or antiquarks) with transverse spin aligned and anti-aligned with the transverse proton spin. The latter quantities are the "transversity" distributions (15, 11, 16, 17) and are denoted $\delta f(x, \mu^2)$ (see Table 1).[2] Note that in the case of transverse polarization a $\cos(2\phi)$ dependence of the cross section on the azimuthal angle ϕ of the observed final-state particle arises (15, 11, 16, 17), since an extra axis is defined by the transverse spin. We also mention that transverse single-spin cross sections, such as $d\sigma_\uparrow^{pp\to\pi X}/d\mathcal{P} - d\sigma_\downarrow^{pp\to\pi X}/d\mathcal{P}$, are allowed to be nonzero in QCD but vanish in the simple parton-model picture presented so far (18, 19) (see Section 5.2).

Extension to polarization in the final state is also possible. If the observed particle in Equation 1 were, say, a Λ-hyperon instead of the (spinless) pion, one could consider the first line of Equation 3 for the helicities of one of the incoming protons (the other proton is assumed to be unpolarized, for simplicity) and of the Λ. In this way one obtains a "helicity transfer" cross section (14) that depends on the distribution of parton f_2 for the unpolarized proton, on Δf_1 for the polarized proton, on polarized fragmentation functions ΔD_f^Λ (defined in analogy with Δf), and on helicity-transfer subprocess cross sections.

For spin experiments, the most important quantity in practice is not the polarized cross section itself, but the spin asymmetry, which is given by the ratio of the polarized over the unpolarized cross section. For our example above, it reads

$$A_{LL}^{\pi} = \frac{d\Delta\sigma^{pp\to\pi X}/d\mathcal{P}}{d\sigma^{pp\to\pi X}/d\mathcal{P}}. \qquad 5.$$

For the asymmetry, one often uses subscripts to denote the type of polarization

[2] One frequently also finds the notation $\Delta_T f(x, \mu^2)$ or $h_1^f(x, \mu^2)$ in the literature.

($L =$ longitudinal, $T =$ transverse) of the initial particles. As follows from Equation 1, the resulting spin asymmetry will possess the generic structure

$$A_{LL} = \frac{\sum_{f_1, f_2, f} \Delta f_1 \times \Delta f_2 \times \left[d\hat{\sigma}^{f_1 f_2 \to f X'} \hat{a}_{LL}^{f_1 f_2 \to f X'} \right] \times D_f}{\sum_{f_1, f_2, f} f_1 \times f_2 \times [d\hat{\sigma}^{f_1 f_2 \to f X'}] \times D_f}, \qquad 6.$$

where $\hat{a}_{LL}^{f_1 f_2 \to f X'} = d\Delta\hat{\sigma}^{f_1 f_2 \to f X'} / d\hat{\sigma}^{f_1 f_2 \to f X'}$ is the spin asymmetry for the subprocess $f_1 f_2 \to f X'$, often also referred to as the analyzing power of the reaction considered. The lowest-order analyzing powers for many reactions interesting at RHIC are depicted in Figure 3.

2.2 Detection

2.2.1 Asymmetries and Errors Asymmetries in a collider experiment can be defined (and measured!) for a single polarized beam or for both beams polarized, with longitudinally polarized beams, transversely polarized beams, or a combination of these. Additionally, one can study a combination of beam spin state and final-state angular dependence. For longitudinal polarization for both beams, the

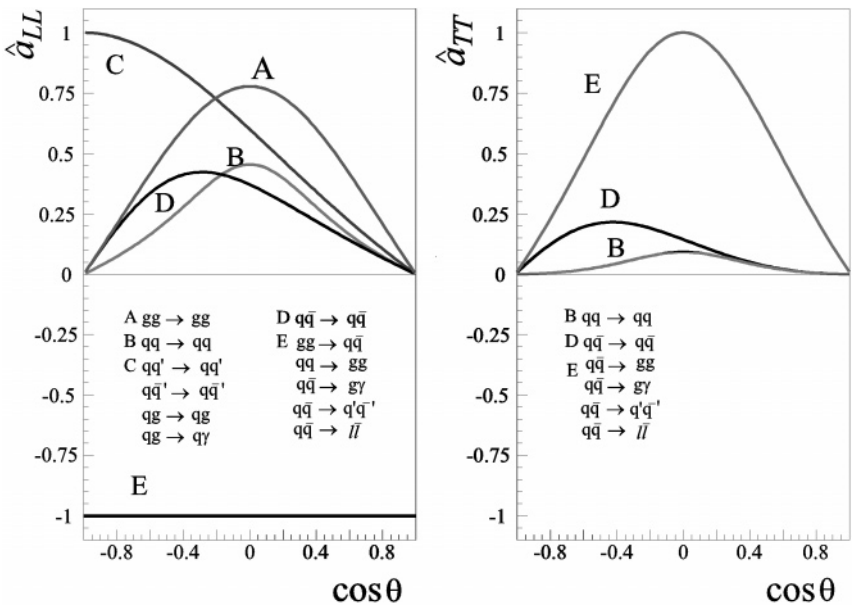

Figure 3 Lowest-order analyzing powers for various reactions relevant for RHIC, as functions of the partonic center-of-mass system (cms) scattering angle (14, 20). *Left:* longitudinal polarization; *right:* transverse polarization [a factor $\cos(2\phi)$ has been taken out, where ϕ is the azimuthal angle of one produced particle].

asymmetry A_{LL} is defined as

$$A_{LL} = \frac{(\sigma_{++} + \sigma_{--}) - (\sigma_{+-} + \sigma_{-+})}{(\sigma_{++} + \sigma_{--}) + (\sigma_{+-} + \sigma_{-+})}. \quad 7.$$

Here, σ_{+-} represents a cross section for producing a specified final state with the initial proton helicities $(+)$ and $(-)$. However, the proton beams are not in pure helicity states. We expect that the beams will be about 70% polarized, meaning that

$$P_{beam} = \frac{B_+ - B_-}{B_+ + B_-} = 0.7, \quad 8.$$

where B_+ refers to the number of protons in the beam with $(+)$ helicity. Therefore, collisions with two bunches of protons, with for example $+0.7$ polarization for one bunch and -0.7 polarization for the other bunch, will include collisions of all four helicity combinations, $(++)$, $(+-)$, $(-+)$, and $(--)$. The experimental asymmetry is defined as follows:

$$A_{LL} = \frac{1}{P_1 P_2} \times \frac{(N'_{++} + N'_{--}) - (N'_{+-} + N'_{-+})}{(N'_{++} + N'_{--}) + (N'_{+-} + N'_{-+})}, \quad 9.$$

where N'_{+-} represents the observed number of events when the beams were polarized $(+)$ for beam 1 and $(-)$ for beam 2, and normalized by the luminosity for the crossing. Here, it is necessary to know only the *relative* luminosity for the $(++)$ and $(--)$ collisions versus the $(+-)$ and $(-+)$ collisions. The beam polarizations are P_1 and P_2. Algebra can confirm that Equation 9 is equivalent to Equation 7.

Similarly, we can define the parity-violating asymmetry for one beam polarized longitudinally,

$$A_L = -\frac{\sigma_+ - \sigma_-}{\sigma_+ + \sigma_-}, \quad A_L = -\frac{1}{P} \times \frac{N'_+ - N'_-}{N'_+ + N'_-}. \quad 10.$$

The parity-violating asymmetry was defined in 1958 to be positive for left-handed production (21). Observed parity-violating asymmetries are therefore typically positive, due to the left-handed weak interaction.

For transverse spin, one- and two-spin asymmetries are defined in analogy with the longitudinal asymmetries above, referred to as A_N and A_{TT}. In this case, the directions $(+)$ and $(-)$ are transverse spin directions of the beam protons, not the helicities. The transverse-spin asymmetries depend on the production angle, θ, and on the azimuthal angle of the scattering, ϕ, as well as other variables. The azimuthal dependence for scattering two spin-1/2 particles is

$$A_{TT} \propto \cos(2\phi) \quad \text{and} \quad A_N \propto \cos(\phi). \quad 11.$$

$\phi = 0$ is defined for scattering in the plane perpendicular to the polarization direction. Typically the beam is polarized vertically, with $(+)$ polarization up, and positive A_N implies more scattering to the left than to the right of the beam direction. The notation A_{NN} is also used for a transverse two-spin asymmetry, where N

refers to beam polarization normal to the scattering plane. A subscript S traditionally designates beam polarization in the transverse direction in the scattering plane.

From Equation 9 or Equation 10 we need to know the beam polarization(s), count the number of signal events for each combination of beam spin directions, and monitor the relative luminosity for the crossings with these combinations of beam spin directions. The statistical error of the measurement is

$$(\Delta A_{LL})^2 = \frac{1}{N P_1^2 P_2^2} - \frac{1}{N} A_{LL}^2. \qquad 12.$$

Here N is the total number of events observed, and it is assumed that the statistical errors on the relative luminosities and on the beam polarization are small. For the single spin asymmetry,

$$(\Delta A_L)^2 = \frac{1}{N P_1^2} - \frac{1}{N} A_L^2. \qquad 13.$$

For small to moderate asymmetries,

$$\Delta A_{LL} = \pm 1/(P_1 P_2) \times \frac{1}{\sqrt{N}} \text{ and } \Delta A_L = \pm 1/P \times \frac{1}{\sqrt{N}}. \qquad 14.$$

Since we expect $P = P_1 = P_2 = 0.7$, 10^4 events would give an error of $\Delta A_{LL} = \pm 0.02$ for the double spin asymmetry, or $\Delta A_L = \pm 0.014$ for the parity-violating asymmetry.

In principle, asymmetry measurements are very straightforward. As long as the detector acceptance remains stable with time between reversals of the beam spin states, the measurement will be stable and the errors will be largely statistical. However, when reversals of the beam polarization are spread apart in time, and/or the beam conditions for opposite spin states differ, acceptance can change and false asymmetries develop. At RHIC the bunches, 120 in each ring, are prepared independently at the source, so that the bunches can alternate polarization sign, 106 ns apart, as shown in Figure 4. Note that one ring with alternate bunches and the other ring with alternating pairs of bunches create the four spin combinations, $(++)$, $(+-)$, $(-+)$, and $(--)$. Therefore, the concern of time-dependent acceptance and beam location variations for opposite sign beams should be negligible at RHIC, and asymmetry measurement errors should be mainly statistical, even for small asymmetries.

What systematic errors do we expect at RHIC? There are two classes of systematic errors: false asymmetries and scale errors. If the relative luminosities for the

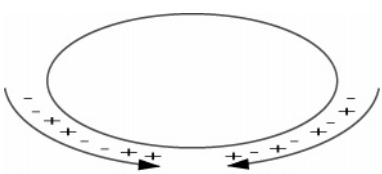

Figure 4 Bunch filling pattern with respect to the spin states of polarized protons.

bunch spin combinations are incorrectly measured through, for example, a saturation effect in the luminosity monitor, which couples to variations in beam intensity for the bunch spin combinations, the numerator of Equation 9 or Equation 10 will be nonzero from the incorrect normalization, creating a false asymmetry. If the beam polarization is incorrect, no false asymmetry is created, but the scale of the resulting asymmetry is changed.

Each experiment will measure the relative luminosities for each crossing. The luminosity monitors must be independent of beam polarization, and statistical errors on the relative luminosity measurements need to be very small to match the statistical sensitivity available for high-statistics measurements, such as jet production.

Relative luminosity needs to be known to the 10^{-4} level for some asymmetry measurements. This job appears daunting, but the time dependence of the acceptance (efficiency is included with acceptance in this discussion) of the luminosity monitor needs to be stable only over roughly one turn of RHIC, or 13 μs.

2.2.2 Polarimetry Polarization is measured by using a scattering process with known analyzing power. Knowledge of the analyzing power for different processes can come from theoretical calculations, for example for QED processes, and from experimental measurements using a beam or target with known polarization. Polarimetry at RHIC (6) will be based on elastic proton-proton and elastic proton-carbon scattering in the Coulomb nuclear interference (CNI) region. The analyzing power there is largely calculable; it is expected to be small but significant. It can be determined to excellent precision using a polarized proton target in RHIC, and the rates for CNI scattering are very high.

Sensitivity to the proton spin is from scattering the Coulomb field of an unpolarized particle (proton or carbon) from the magnetic moment of the polarized proton. This method uses the dominance of the interference of the one-photon exchange helicity-flip electromagnetic amplitude, proportional to the proton anomalous magnetic moment, with the non-flip strong hadronic amplitude, which is determined by the pp or pC total cross section σ_{tot} (22–26). However, there can also be a hadronic spin-flip term, which is not presently calculable. (This possibility is discussed in more detail in Section 7.) Therefore, significant sensitivity to the proton spin is predicted over the entire RHIC energy range from the electromagnetic term, but the absolute sensitivity is limited to $\pm 15\%$ (25). For this reason, a polarized hydrogen gas jet target will be installed at RHIC. The polarization of the jet target can be measured to $\pm 3\%$ so that the analyzing power in the CNI region can be measured precisely, and this analyzing power will then be used to determine the beam polarization at RHIC precisely.

Existing polarized hydrogen gas jet targets are thin, so that the determination of the beam polarization using the jet target will take hours. For this reason, RHIC will also use carbon ribbon targets and use proton-carbon CNI scattering to monitor the beam polarization frequently.

Absolute beam polarization is expected to be known to $\pm 5\%$. The systematic scale uncertainty of the asymmetry measurements will be of the order of $\pm 5\%$

for single spin measurements such as Equation 10 and ±10% for two spin measurements such as Equation 9. By scale uncertainty we mean that in forming the ratio of the error in the asymmetry measurement, ΔA_{LL} in Equation 14, to the measurement itself, A_{LL} in Equation 9, the polarization normalization divides out. Therefore, the polarization uncertainty applies to the scale of the measurement and not to the statistical significance of the measurement.

2.2.3 RHIC Detectors This article emphasizes the physics that will be probed at RHIC-Spin. There are six collision points at RHIC, as shown in Figure 1, and two are used for the two large detectors, PHENIX (27) and STAR (28). These detectors are quite complementary: STAR emphasizes large coverage with tracking, and the strengths of PHENIX are in fine-grained calorimetry for photons and electrons and in "forward" muon detectors. Sensitivities for the spin measurements at RHIC are based on these detectors. Although one could discuss the sensitivity for a 4π-acceptance fine-grained detector, such a detector does not exist. And we note that, for example, the PHENIX electromagnetic calorimeter (EMCal) has 100 times finer granularity than previous collider detectors. The PP2PP (29) and BRAHMS (30) detectors share one collision point, and the PHOBOS (31) detector is located at another crossing. STAR and PHENIX will measure gluon and quark polarizations with hard scattering. The PP2PP experiment will measure spin dependence in small-angle elastic scattering; BRAHMS and PHOBOS will measure transverse spin asymmetries.

The PHENIX detector, shown in Figure 5, has two central arms at 90° to the beams with fine-grained EMCal towers, $\Delta\eta \times \Delta\phi = 0.01 \times 0.01$. The minimum opening angle for $\pi^0 \rightarrow \gamma\gamma$ corresponds to one tower for a 30-GeV π^0. This is important to separate directly produced photons, a probe of gluon polarization, from background from π^0 decay. Resolution is excellent, with $\Delta E/E = \pm 3\%$ at 10 GeV. The two central arms each cover 90° in azimuth, left and right. Pseudorapidity acceptance is $|\eta| < 0.35$. The vertex detector, central tracker, ring-imaging Cherenkov detector (RICH), and time expansion chamber (TEC) are also shown. The central magnetic field, provided by two Helmholtz coils, is 0.8 Tesla meters, integrated radially. The tracking p_T resolution is $\Delta p_T/p_T = \pm 2.5\%$ at 10 GeV/c for the east arm, which includes the TEC, and ±5% in the west arm without a TEC. Triggering in the central arms, for selection of high-p_T direct photons, electrons, and charged pions, will be based on overlapping tower clusters in the EMCal, combined with RICH information. Studies indicate a sufficiently clean and efficient electron trigger to allow $p_T > 1$ GeV/c or so. Such a low-momentum electron trigger is attractive to obtain charm quark events.

The PHENIX muon arms surround the beams, covering $\Delta\phi = 2\pi$ and $1.2 < |\eta| < 2.4$. The arms include a muon identifier (MuID) with five iron-detector layers, as well as three tracking stations. The muon arm magnets produce a radial field, ranging from 0.2 to 0.75 Tesla meters, integrated along the beam direction. Longitudinal momentum resolution is about ±2% at 10 GeV/c. A 4-GeV/c muon penetrates to the fifth MuID layer.

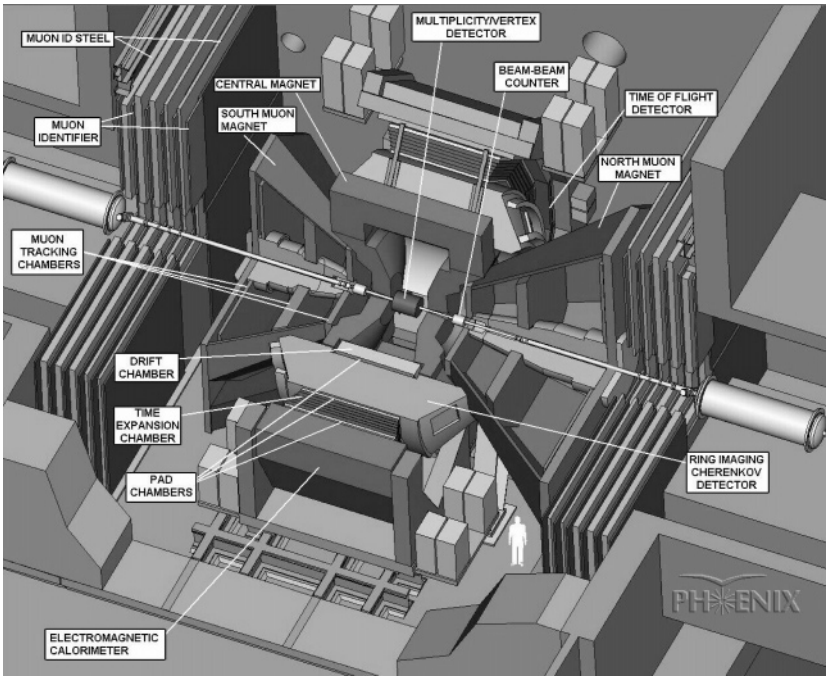

Figure 5 The PHENIX detector system.

PHENIX will emphasize muon measurements for $W \rightarrow \mu\nu$, Drell-Yan lepton pairs, J/ψ, and heavy flavors. Central arms will measure γ, jet fragmentation to $\pi^{0,\pm}$, and $W \rightarrow e\nu$, as well as heavy flavors (single lepton, and e with μ), with small acceptance and high granularity.

The STAR detector is shown schematically in Figure 6. A barrel time projection chamber (TPC) covers $|\eta| < 1.0$ and $\Delta\phi = 2\pi$. This is surrounded by an EMCal with towers $\Delta\eta \times \Delta\phi = 0.05 \times 0.05$. The EMCal has a shower maximum detector at a depth of five radiation lengths with projective readout wire chambers reading longitudinally and azimuthally, each with 1-cm spacing. Studies show an effective separation of single photons from merged photons from π^0 decay out to $p_T = 25$ GeV/c. Energy resolution is excellent, with $\Delta E/E = \pm 5\%$ at 10 GeV. Additional barrel detection includes a silicon drift vertex tracker around the collision point and an array of trigger counters outside the TPC. The central solenoid field is 1.0 Tesla meters, integrated radially. The STAR p_T resolution is $\pm 3\%$ at $p_T = 10$ GeV/c. STAR is also building one endcap calorimeter to cover $1 < \eta < 2$ for photons and electrons and to expand the jet cone coverage.

Triggering at STAR will be based on the trigger counters and EMCal, which are fast detectors. A major issue to resolve is the long memory of the TPC, which will include on the order of 800 out-of-time tracks from the 40-μs drift time, at full

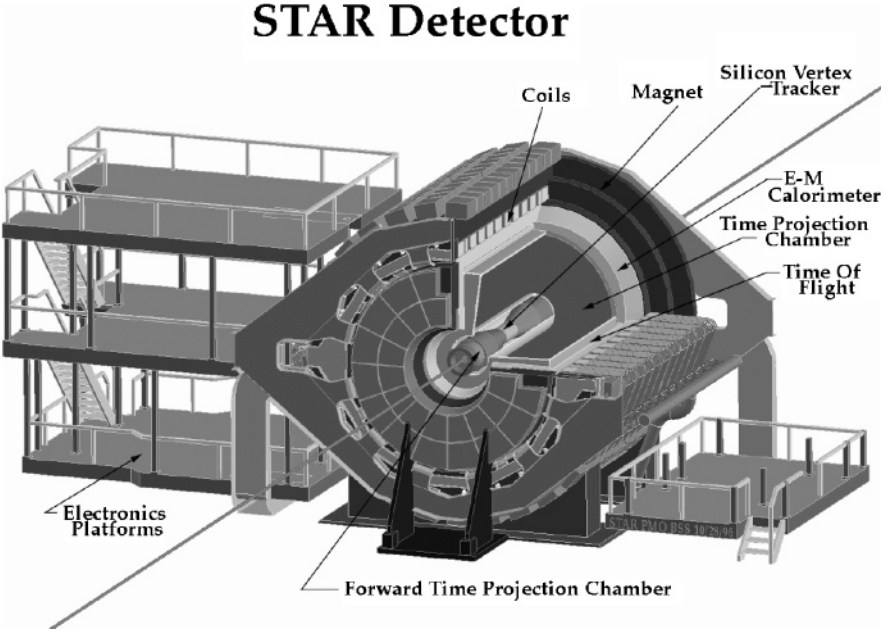

Figure 6 Cut view of STAR detector system.

luminosity with a 10-MHz collision rate. STAR studies have shown that the drift of the out-of-time tracks cause them to point significantly away from the collision point. This drift will be used to remove the unwanted tracks, and this must be done before writing to tape. Studies have also shown good jet reconstruction after the tracks are removed. Jets will be reconstructed at STAR with a combination of EMCal and tracking, with no hadronic calorimetry. Simulations show a full width at half maximum of 30% for the $\Delta p_{jet}/p_{jet}$ distribution, limited by the hadronization dynamics of final-state partons. A cone size of $R = \sqrt{\Delta\eta^2 + \Delta\phi^2} = 0.7$ was used. STAR will measure jets, $\gamma + jet$, and $W \rightarrow e\nu$, with wide acceptance and reconstruction of the parton kinematics.

The PP2PP experiment is designed to study small-angle proton-proton elastic scattering, from $-t = 0.0005$ to $-t = 1.5$ (GeV/c)^2. Silicon-strip detectors will be placed in Roman pots at two locations along each beam to measure scattering to very small angles. The experiment will also use a polarized hydrogen jet target with silicon recoil detectors to cover lower center-of-mass energy and will measure the absolute polarization of the RHIC beams.

The BRAHMS detector has two movable spectrometers ($2.3^\circ \leq \theta \leq 30^\circ$ and $30^\circ \leq \theta \leq 95^\circ$) with superb particle identification. The spectrometer covers up to 30 GeV/c with $\Delta p/p = \pm 0.1\%$ and it will provide unique measurements of single transverse-spin asymmetries in the forward, thus high-x_F, region.

PHOBOS is a table-top–sized detector that uses silicon-strip detectors to cover a large solid angle. Two spectrometers comprise 15 planes of silicon pad detectors each, with seven planes in a 2-Tesla magnetic field. Its wide geometrical acceptance and momentum resolution is suitable for pair or multiparticle final states in spin physics, such as $\rho^0 \to \pi^+\pi^-$.

3. MEASURING Δg AT RHIC

Measurement of the gluon polarization in a polarized proton is a major emphasis and strength of RHIC-Spin. By virtue of the spin sum rule (2), a large Δg is an exciting possible implication (2) of the measured (1) smallness of the quark and antiquark contribution to the proton spin. A large gluon polarization would imply unexpected dynamics in the proton's spin structure. Because of this special importance of Δg, and since it is left virtually unconstrained by the inclusive-DIS experiments performed so far (see Appendix), several experiments focus on its measurement. A fixed-target DIS experiment, HERMES, measures the process $\vec{e}(\vec{\gamma})\,\vec{p} \to h^+h^-X$ (32), where $h = \pi, K$, which is in principle sensitive to the gluon polarization. However, the transverse momenta are low, making interpretation in a hard-scattering formalism difficult. The DIS experiment COMPASS (see e.g. Reference 33) will measure the same reaction at higher energies, as well as heavy-flavor production, to access gluon polarization. Scaling violations and the reaction $\vec{e}(\vec{\gamma})\,\vec{p} \to \text{jet(s)}X$ will constrain Δg at HERA, if the proton ring is polarized (34). At RHIC, the gluon polarization will be measured directly, precisely, and over a large range of gluon momentum fraction, with large momentum transfer ensuring the applicability of perturbative QCD to describe the scattering, and with several independent processes. The RHIC probes, shown in Figure 7, are as follows:

- High-p_T ("prompt") photon production $\vec{p}\,\vec{p} \to \gamma X$
- Jet production, $\vec{p}\,\vec{p} \to \text{jet(s)}X$
- Heavy-flavor production, $\vec{p}\,\vec{p} \to c\bar{c}X, b\bar{b}X$

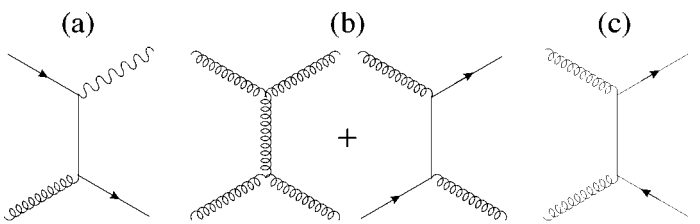

Figure 7 Selected lowest-order Feynman diagrams for elementary processes with gluons in the initial state in pp collisions: (*a*) quark-gluon Compton process for prompt-photon production, (*b*) gluon-gluon and gluon-quark scattering for jet production, and (*c*) gluon-gluon fusion producing a heavy quark pair.

3.1 Prompt-Photon Production

Prompt-photon production, pp, $p\overline{p}$, $pN \to \gamma X$ (35), has been *the* classical tool for determining the unpolarized gluon density at intermediate and large x. At leading order, a photon in the final state is produced in the reactions $qg \to \gamma q$ (Figure 7*a*) and $q\overline{q} \to \gamma g$. Proton-proton, as opposed to proton-antiproton, scattering favors the quark-gluon Compton process, since the proton's antiquark densities are much smaller than the quark ones. The analyzing power for direct photon production is large (Figure 3). Photons produced in this way through partonic hard scattering show a distinct signal at colliders, that of an isolated single photon without jet debris nearby. The production of photons with polarized beams at RHIC is therefore a very promising method to measure Δg (36–39).

If parton kinematics can be approximately reconstructed, one can bin the events in the parton momentum fractions x_1, x_2 of the hard scattering. Assuming dominance of the Compton process, the asymmetry A_{LL} for prompt-photon production can then be written as

$$A_{LL} \approx \frac{\Delta g(x_1)}{g(x_1)} \cdot \left[\frac{\sum_q e_q^2 \left[\Delta q(x_2) + \Delta \overline{q}(x_2) \right]}{\sum_q e_q^2 \left[q(x_2) + \overline{q}(x_2) \right]} \right] \cdot \hat{a}_{LL}(gq \to \gamma q) + (1 \leftrightarrow 2). \quad 15.$$

As a result of the quark charge-squared weighting, the second factor in Equation 15 coincides, to lowest order, with the spin asymmetry A_1^p measured in polarized DIS, and the partonic asymmetry $\hat{a}_{LL}$ is calculable in perturbative QCD. Thus, from the measurement of A_{LL}, one can directly extract $\Delta g(x)/g(x)$.

Both PHENIX and STAR intend to use this procedure for a direct leading-order determination of Δg, where one exploits the dominance of $2 \to 2$ ($ab \to \gamma c$) parton scattering when reconstructing x_1, x_2. This is done either on average based on the detector acceptance for the photon, or event-by-event by observing photon-plus-jet events (STAR). Estimates of the "background" from $q\overline{q}$ annihilation have been made (40). Eventually, the aim will be a "global" QCD analysis of polarized prompt photon, and other RHIC and DIS, asymmetry data to determine the full set of polarized parton densities simultaneously, as is done routinely in the unpolarized case (41, 42, 43). In this case, one can directly work from the spin asymmetries, and inclusion of, for instance, higher-order corrections is more readily possible.

Figure 8 shows the level of accuracy STAR can achieve (40) in a direct measurement of Δg based on reconstructing parton kinematics in photon-plus-jet events. The solid lines show in each plot the input density employed for $\Delta g(x)$, taken from Reference 44. The data points and the error bars show the reconstructed $\Delta g(x)$ and its precision for standard luminosities in runs at $\sqrt{s} = 200$ GeV (open circles) and $\sqrt{s} = 500$ GeV (solid circles).

High-p_T photons can also be produced through a fragmentation process, in which a parton, scattered or produced in a QCD reaction, fragments into a photon plus a number of hadrons. The need for introducing a fragmentation contribution is physically motivated by the fact that a QCD hard-scattering process may

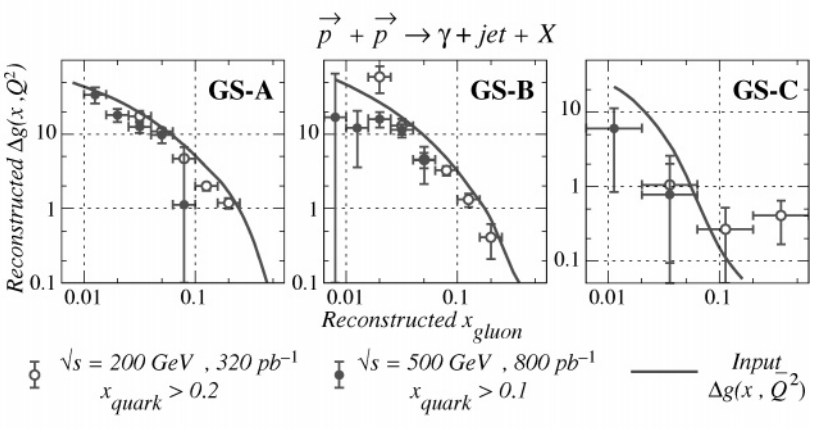

Figure 8 Sensitivity of STAR measurements of $\Delta g(x)$ in the channel $\vec{p}\vec{p} \rightarrow \gamma + \text{jet} + X$.

produce, again through a fragmentation process, a ρ meson that has the same quantum numbers as the photon and can thus convert into a photon, leading to the same signal. In addition, at higher orders, the perturbatively calculated direct component contains divergencies from configurations where a final-state quark becomes collinear to the photon. These singularities naturally introduce the need for nonperturbative fragmentation functions into which they can be absorbed. So far, the photon fragmentation functions are insufficiently known; information is emerging from the LEP experiments (45). Note that all QCD partonic reactions contribute to the fragmentation component; thus, the benefit of having a priori only one partonic reaction ($q\overline{q} \rightarrow \gamma g$) competing with the signal ($qg \rightarrow \gamma q$) is lost, even though some of the subprocesses relevant to the fragmentation part at the same time result from a gluon initial state. Theoretical studies (46–49) for photon production in unpolarized collisions, based on predictions (46, 50, 51) for the photon-fragmentation functions that are compatible with the sparse LEP data, indicate that the fragmentation component is in practice a small, albeit nonnegligible, effect.

In the fixed-target regime, fragmentation photons are believed (48) to contribute at most 20% to the direct photon cross section. At collider energies, the fragmentation mechanism is estimated to produce about half of the observed photons; however, an "isolation" cut can be imposed on the photon signal in experiment. Isolation is an experimental necessity: In a hadronic environment, the study of photons in the final state is complicated by the abundance of π^0s, which decay into pairs of γs. If two photons are unambiguously detected in an event, their invariant mass can indicate whether they resulted from a π^0 (or η) decay. However, either escape of one of the decay photons from the detector or merging of the two photons from π^0 decay at high p_T fake a single photon event. The isolation cut reduces this background, since π^0s are embedded in jets. If a given neighborhood of the

photon is free of energetic hadron tracks, it is less likely that the observed photon came from π^0 decay, and the event is kept; it is rejected otherwise. Traditionally, isolation is realized by drawing a cone of fixed aperture in φ–η space around the photon [where φ is the photon's azimuthal angle and $\eta = -\ln\tan(\theta/2)$ is its pseudorapidity, defined through its polar angle θ], and by restricting the hadronic transverse energy allowed in this cone to a certain small fraction of the photon transverse energy. In this way, the fragmentation contribution to single γs, resulting from an essentially collinear process, will also be diminished (52). It is not expected (47, 48) that fragmentation will remain responsible for more than 15–20% of the photon signal after isolation. It has been suggested (53) that allowing proportionally less hadronic energy the closer to the photon it is deposited, rather than permitting a fixed fraction in the full isolation cone, would improve isolation by reducing the fragmentation photons still further.

Several early theoretical studies for isolated prompt-photon production at polarized RHIC have been published (e.g. 36–39). The QCD corrections to the direct (i.e. nonfragmentation) component of polarized prompt-photon production were first calculated in References 54 and 55 and are now routinely included in theoretical studies (e.g. 56–60). In particular, References 58, 59, and 60 present Monte Carlo codes for the next-to-leading-order (NLO) corrections to the direct part of the cross section, which allow the isolation constraints to be taken into account and also have the flexibility to predict photon-plus-jet observables, $\vec{p}\,\vec{p} \to \gamma + jet + X$. We also emphasize that much effort has gone, and is still going, into event-generator studies (40, 61–63) for prompt-photon physics at RHIC.

Figure 9 shows the asymmetry as obtained in an NLO theory calculation, as a function of the photon's transverse momentum p_T. A rapidity cut $|\eta| < 0.35$ has been applied, matching the acceptance of the PHENIX experiment. In the left (right) part of the figure we plot the asymmetries obtained at $\sqrt{s} = 200$ GeV (500 GeV). The isolation of Reference 53 was used, with isolation cone opening $R_0 = 0.4$ and $\epsilon_\gamma = 1, n = 1$ (see Reference 53 for details on the latter parameters). The solid, dashed, and dotted lines correspond to the NLO predictions obtained with GRSV-STD, GRSV-MAXg (64), and GS-C (44) polarized parton densities, respectively. These densities are all compatible with present data from polarized DIS and differ mainly in their gluon content: GRSV-MAXg has a very sizeable positive gluon distribution, whereas GS-C has a small, and oscillating, Δg. The gluon of GRSV-STD lies between the other two. The three gluon densities are shown in Figure 22 in the Appendix. The error bars represent the expected statistical accuracy for the measurement at PHENIX, with $\Delta\phi = \pi$ and for standard luminosities and beam polarizations.

It is a striking feature of Figure 9 that different spin-dependent gluon densities do indeed lead to very different spin asymmetries for prompt-photon production. RHIC experiments will be able to measure Δg.

For fixed p_T, higher-energy probes lower x in the parton distributions, and this leads to the smaller predicted asymmetries for $\sqrt{s} = 500$ GeV. If one considers

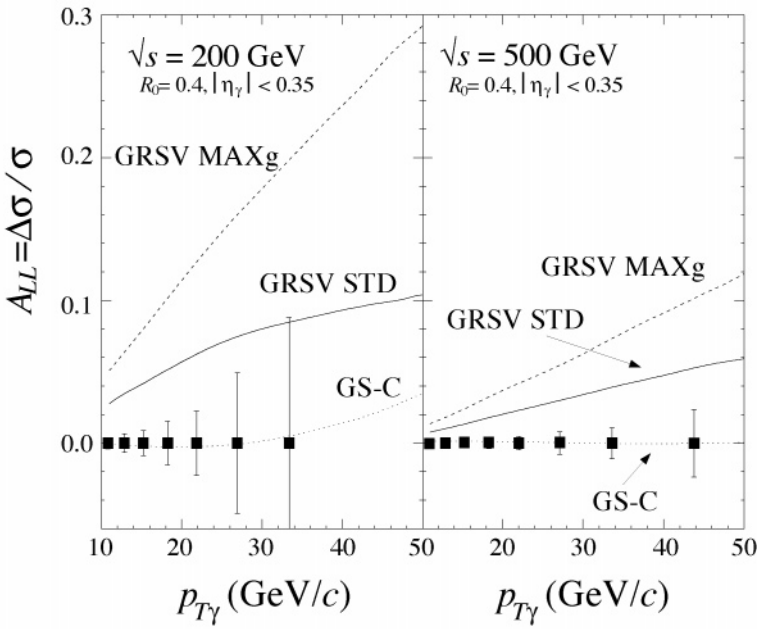

Figure 9 Asymmetry as a function of transverse momentum, for various polarized parton densities, at different cms energies (60). The expected statistical errors for the PHENIX experiment are also shown.

the same $x_T = 2p_T/\sqrt{s}$ value for the two energies in Figure 9, the parton densities are being probed at similar momentum fractions but rather different "resolution" scales, of the order of p_T. It will be interesting to see whether measurements performed at different center-of-mass system (cms) energies will yield information that is consistent, and compatible, with QCD evolution.

Present comparisons between theory and experiment [and possibly between experiment and experiment (49)] regarding unpolarized direct γ production are unsatisfactory (65). Transverse smearing of the momenta of the initial partons participating in the hard scattering, substantially larger than that already introduced by the NLO calculation, has been considered (66, 41, 67) to reconcile theory with data. This approach is partly based on measured values of dimuon, dijet, and diphoton pair transverse momenta k_T in hadronic reactions (66) and has enjoyed some phenomenological success. More recently, the role of all-order-resummations of large logarithms in the partonic cross section, generated by (multiple) soft-gluon emission, has been investigated in the context of prompt-photon production (68–71). Threshold resummations (69) have been shown (70) to lead to improvements in the fixed-target regime, and a very recent new formalism (71) that jointly incorporates threshold and k_T resummations has the potential of creating the substantial enhancements needed for bringing theory into agreement

with data. It is likely that a better understanding of the prompt-photon process will have been achieved by the time RHIC performs the first measurements of $\vec{p}\vec{p} \rightarrow \gamma X$. Also, the main problems reside in the fixed-target region; at colliders there is much less reason for concern. RHIC itself should also be able to provide new and complementary information in the unpolarized case—never before have prompt-photon data been taken in pp collisions at energies as high as $\sqrt{s} = 200$–500 GeV.

Finally, we note that it was also proposed (37, 72, 73) to determine Δg through the reaction $qg \rightarrow \gamma^* q$, which is again the Compton process, but now with a photon off-shell by the order of a few GeV and giving rise to a Drell-Yan lepton pair of comparable p_T. The advantage is a cleaner theoretical description; for instance, no photon fragmentation component is present in this case. However, compared to prompt-photon production at a given p_T, the event rate is reduced by 2–3 orders of magnitude due to the additional factor $\alpha_{em}/(3\pi Q^2)$ in the Drell-Yan cross section, where Q is the dilepton mass. Higher statistics are available at lower p_T, but at the price of reduced asymmetry and higher background from $q\overline{q} \rightarrow \gamma^* g$ annihilation.

3.2 Jet Production

Toward the higher end of RHIC energies, jets could be the key to Δg: At $\sqrt{s} = 500$ GeV, clearly structured jets will be copiously produced, and jet observables will show a strong sensitivity to Δg thanks to the dominance (74, 39) of the gg and qg initiated subprocesses (see Figure 7*b*) in accessible kinematical ranges. Jet studies will be performed by STAR. One can alternatively look for high-p_T leading hadrons such as $\pi^0, \pi^{\pm}$, whose production proceeds through the same partonic subprocesses but involves an explicit fragmentation function in the theoretical description. This is planned for the PHENIX experiment, where the limitation in angular coverage precludes jet studies.

Knowledge of the NLO QCD corrections is expected to be particularly important for the case of jet production, since it is only at NLO that the QCD structure of the jet starts to play a role in the theoretical description, providing for the first time the possibility of realistically matching the procedures used in experiment in order to group final-state particles into jets. The task of calculating the NLO QCD corrections to polarized jet production has been accomplished (75). Furthermore, a Monte Carlo code that had been designed by Frixione (76), based on Reference 77 and the subtraction method in hadron-hadron unpolarized collisions, was extended to the polarized case in Reference 75. We emphasize that in the unpolarized case, the comparison of NLO theory predictions with jet production data from the Tevatron is extremely successful (see e.g. Reference 78).

Figure 10 shows the double-spin asymmetry for single-inclusive jet production at NLO as a function of the jet p_T and for various polarized parton densities (44, 64, 79) with different Δg (see Figure 22 in the Appendix). A cut $|\eta| < 1$ has been applied, and we have chosen the Ellis-Soper (ES) cluster jet algorithm (80)

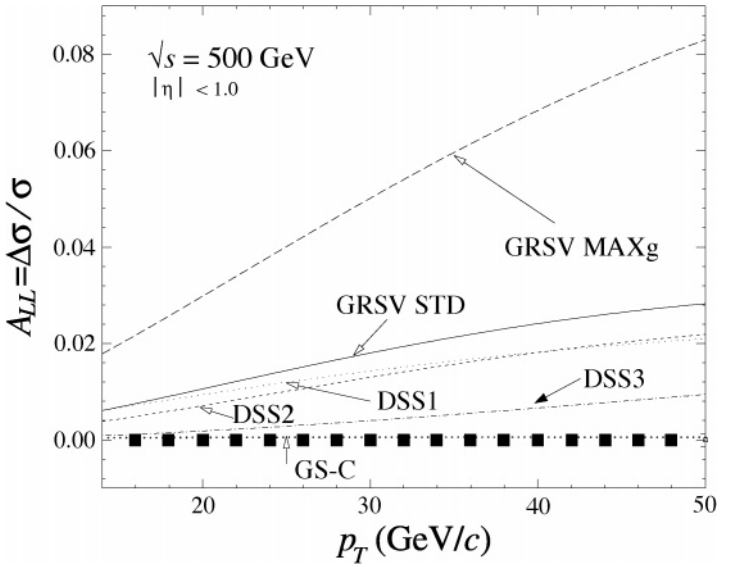

Figure 10 Asymmetry versus jet transverse momentum (75) for various polarized parton density sets. The "data point" for $p_T = 48\,\mathrm{GeV}/c$ indicates the statistical accuracy expected for the STAR experiment for standard polarization and luminosity. Expected errors for lower p_T are smaller than the points shown.

with the resolution parameter $D = 1$. The renormalization and factorization scales have been chosen as $\mu_0 \approx p_T$ (for further details, see Reference 75). The asymmetry shows a strong sensitivity to Δg. However, the asymmetry is rather small, regardless of the specific parton densities used. Fortunately, the expected statistical accuracy of such a jet measurement, calculated for standard luminosity and indicated in the figure, is very good.

The inclusion of NLO corrections in jet production, as shown in Figure 11, leads to a clear reduction in scale dependence of the cross section. One thereby gains confidence that it is possible to calculate reliably the cross section and the spin asymmetry for a given Δg. This reduction in scale dependence after NLO corrections is also seen for direct photon production (60).

3.3 Heavy-Flavor Production

The production of heavy quark pairs in hadronic collisions is dominated by gluon-gluon fusion, $gg \to Q\overline{Q}$ (see Figure 7*c*). For pp collisions, the competing channel $q\overline{q} \to Q\overline{Q}$ is particularly suppressed, since it requires an antiquark in the initial state. Thus, heavy quarks provide direct access to the gluons in the proton. Early predictions (81) at the lowest order demonstrated that indeed this reaction could

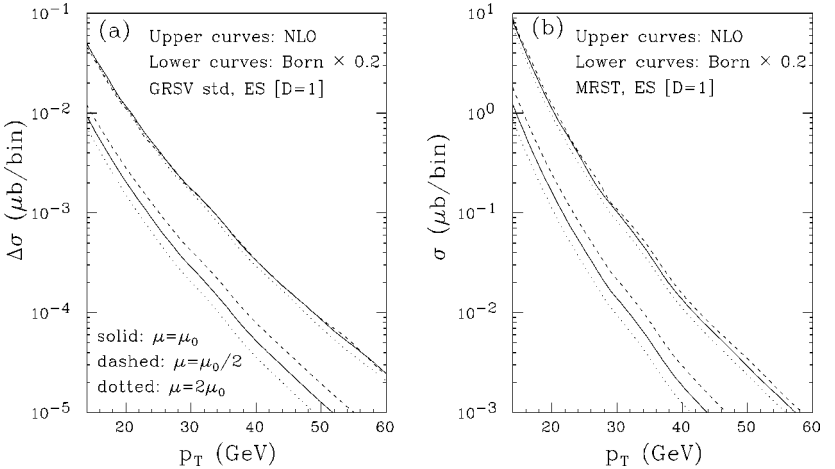

Figure 11 Scale dependence of the next-to-leading-order and Born p_T distributions for jet production (75). (*a*) Polarized pp scattering and (*b*) unpolarized pp scattering at $\sqrt{s} =$ 500 GeV. The range of the pseudorapidity is restricted to $|\eta| < 1$.

be used to measure Δg in polarized pp collisions. The importance of NLO corrections for a quantitative analysis was pointed out (82). Presently, only the NLO QCD corrections to heavy-flavor production in polarized photon-photon (83) and photon-proton (84, 85) collisions are known; it is anticipated that the full set of NLO corrections relevant for polarized pp collisions will be available soon (86). It should be mentioned that in the unpolarized case, theoretical NLO predictions for hadro- and photoproduction of heavy flavors often fail to provide a satisfactory description of the data (see Reference 87 for review).

Heavy-flavor production can be selected by the channels $pp \to \mu^{\pm} X$, $pp \to e^{\pm} X$, $pp \to \mu^{+}\mu^{-} X$, $pp \to e^{+}e^{-} X$, and $pp \to \mu^{\pm} e^{\mp} X$. Like-sign leptons are also possible from bottom, with one direct *b*-decay to a lepton and one sequential decay through charm. Charm and bottom events will probe the gluon density at different momentum fractions and scales and also enter the analysis with different, albeit calculable, weights. Experimentally it may be possible to determine the fraction of the charm production rate by, for example, looking at the channel $pp \to \mu^{+} D^{0} X$.

The production of heavy quarkonia is another potentially attractive probe of the gluon density with a clear experimental signature. However, so far we do not understand the production mechanism. Predictions for ψ production based on the color-singlet model (88) fall short of experimental data taken at the Tevatron (see e.g. Reference 89). This has stimulated the development of a more general approach that also gives rise to potentially important color-octet contributions (90). Theoretical studies for the spin asymmetry in charmonium production in pp collisions have been presented (91, 81, 92–94). Reference 92 considers the color-singlet

mechanism; Reference 93 also examines color-octet contributions. Sensitivity to the production mechanism as well as to Δg is found. Similarly, $\chi_2(3556)$ production at RHIC would have the potential to discriminate between the color-singlet and the color-octet mechanisms, as well as to pin down Δg (94). Here, one would have to look at the angular distribution of the decay photon in $\chi_2 \rightarrow J/\psi + \gamma$. The number of observed events for this reaction will unfortunately be low at RHIC.

4. QUARK AND ANTIQUARK HELICITY DISTRIBUTIONS

Measurements in polarized DIS (1), when combined with information from baryon octet β-decays (2), show that the total quark-plus-antiquark contribution to the proton's spin, summed over all flavors, is surprisingly small. In the standard interpretation of the β-decays (2), this finding is equivalent to evidence for a large negative polarization of strange quarks in the proton, which makes it likely that also the $SU(2)(u, d)$ sea is strongly negatively polarized. This view is corroborated by the fact that in this analysis the spin carried, for example, by u quarks comes out much smaller than generally expected in quark models (2), implying that a sizeable negative u-sea polarization partly compensates that of the valence u quarks. Alternative treatments of the information from β-decays (95, 64), when combined with the DIS results, also directly yield large negative $\overline{u}$ and $\overline{d}$ polarizations. Inclusive DIS (through γ^* exchange) itself is sensitive to the combined contributions of quarks and antiquarks of each flavor but cannot provide information on the polarized quark and antiquark densities separately (see Appendix). Directly measuring the individual polarized antiquark distributions is therefore an exciting task and will also help to clarify the overall picture concerning DIS and the β-decays.

Further motivation for dedicated measurements of antiquark densities comes from unpolarized physics. Experiments in recent years have shown (96–98) a strong breaking of $SU(2)$ symmetry in the antiquark sea, with the ratio $\overline{d}(x)/\overline{u}(x)$ rising to 1.6 or higher. It is very attractive to learn whether the polarization of $\overline{u}$ and $\overline{d}$ is large and asymmetric as well. RHIC experiments will measure the $\overline{d}/\overline{u}$ unpolarized ratio and the $\overline{u}$ and $\overline{d}$ polarizations separately.

Semi-inclusive DIS measurements (99) are one approach to achieving a separation of quark and antiquark densities. This method combines information from proton and neutron (or deuteron) targets and uses correlations in the fragmentation process between the type of leading hadron and the flavor of its parton progenitor, expressed by fragmentation functions. The dependence on the details of the fragmentation process limits the accuracy of this method. At RHIC the polarization of the $u, \overline{u}, d$, and $\overline{d}$ quarks in the proton will be measured directly and precisely using maximal parity violation for production of W bosons in $u\overline{d} \rightarrow W^+$ and $d\overline{u} \rightarrow W^-$ (14, 100–103). In addition, at RHIC, inclusive production of π, K, and Λ will be used to measure quark and antiquark polarization through the

fragmentation process. Another probe at RHIC will be Drell-Yan production of lepton pairs (104, 38, 39, 105, 106, 102, 103).

4.1 Weak Boson Production

Within the standard model, W bosons are produced through pure V-A interaction. Thus, the helicities of the participating quark and antiquark are fixed in the reaction. In addition, the W couples to a weak charge that correlates directly to flavors, if we concentrate on one generation. Indeed the production of Ws in pp collisions is dominated by u, d, $\overline{u}$, and $\overline{d}$, with some contamination from s, c, $\overline{s}$, and $\overline{c}$, mostly through quark mixing. Therefore W production is an ideal tool to study the spin-flavor structure of the nucleon.

The leading-order production of Ws, $u\overline{d} \rightarrow W^+$, is illustrated in Figure 12. The longitudinally polarized proton at the top of each diagram collides with an unpolarized proton, producing a W^+. At RHIC the polarized protons will be in bunches, alternately right- (+) and left- (−) handed. The parity-violating asymmetry is the difference of left-handed and right-handed production of Ws, divided by the sum and normalized by the beam polarization:

$$A_L^W = \frac{1}{P} \times \frac{N_-(W) - N_+(W)}{N_-(W) + N_+(W)}. \qquad 16.$$

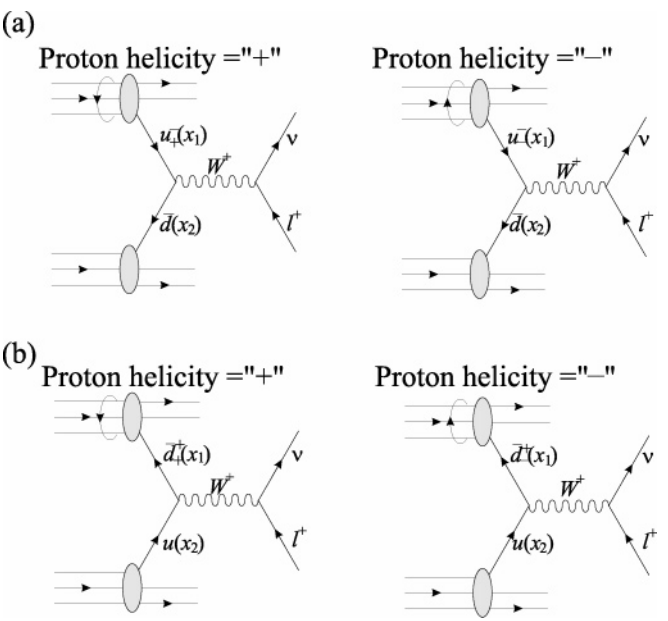

Figure 12 Production of a W^+ in a $\vec{p}p$ collision, at lowest order. (*a*) Δu is probed in the polarized proton. (*b*) $\Delta\overline{d}$ is probed.

As Figure 4 shows, we can construct this asymmetry from either polarized beam, and by summing over the helicity states of the other beam. The production of the left-handed weak bosons violates parity maximally. Therefore, if for example the production of the W^+ proceeded only through the diagram in Figure 12*a*, the parity-violating asymmetry would directly equal the longitudinal polarization asymmetry of the u quark in the proton:

$$A_L^{W^+} = \frac{u_-^-(x_1)\bar{d}(x_2) - u_+^-(x_1)\bar{d}(x_2)}{u_-^-(x_1)\bar{d}(x_2) + u_+^-(x_1)\bar{d}(x_2)} = \frac{\Delta u(x_1)}{u(x_1)}. \qquad 17.$$

Similarly, for Figure 12*b* alone,

$$A_L^{W^+} = \frac{\bar{d}_-^+(x_1)u(x_2) - \bar{d}_+^+(x_1)u(x_2)}{\bar{d}_-^+(x_1)u(x_2) - \bar{d}_+^+(x_1)u(x_2)} = -\frac{\Delta\bar{d}(x_1)}{\bar{d}(x_1)}. \qquad 18.$$

In general, the asymmetry is a superposition of the two cases:

$$A_L^{W^+} = \frac{\Delta u(x_1)\bar{d}(x_2) - \Delta\bar{d}(x_1)u(x_2)}{u(x_1)\bar{d}(x_2) + \bar{d}(x_1)u(x_2)}. \qquad 19.$$

To obtain the asymmetry for W^-, one interchanges u and d.

For the pp collisions at RHIC with $\sqrt{s} = 500$ GeV, the quark will be predominantly a valence quark. By identifying the rapidity of the W, y_W, relative to the *polarized* proton, we can obtain direct measures of the quark and antiquark polarizations, separated by quark flavor: $A_L^{W^+}$ approaches $\Delta u/u$ in the limit of $y_W \gg 0$, whereas for $y_W \ll 0$ the asymmetry becomes $-\Delta\bar{d}/\bar{d}$. Higher-order corrections change the asymmetries only a little (102, 103).

The kinematics of W production and Drell-Yan production of lepton pairs is the same. The momentum fraction carried by the quarks and antiquarks, x_1 and x_2 (without yet assigning which is which), can be determined from y_W,

$$x_1 = \frac{M_W}{\sqrt{s}}e^{y_W}, \quad x_2 = \frac{M_W}{\sqrt{s}}e^{-y_W}. \qquad 20.$$

Note that this picture is valid for the predominant production of Ws at $p_T = 0$. The experimental difficulty is that the W is observed through its leptonic decay $W \to l\nu$, and only the charged lepton is observed. We therefore need to relate the lepton kinematics to y_W, so that we can assign the probability that the polarized proton provided the quark or antiquark. Only then will we be able to translate the measured parity-violating asymmetry into a determination of the quark or antiquark polarization in the proton.

The rapidity of the W is related to the lepton rapidity in the W rest frame (y_l^*) and in the lab frame ($y_l^{\rm lab}$) by

$$y_l^{lab} = y_l^* + y_W, \quad \text{where } y_l^* = \frac{1}{2}\ln\left[\frac{1+\cos\theta^*}{1-\cos\theta^*}\right]. \qquad 21.$$

Here θ^* is the decay angle of the lepton in the W rest frame, and $\cos\theta^*$ can be determined from the transverse momentum (p_T) of the lepton with an irreducible uncertainty of the sign (107), since

$$p_T^{\text{lepton}} = p_T^* = \frac{M_W}{2}\sin\theta^*. \qquad 22.$$

In this reconstruction, the p_T of the W is neglected. In reality, it has a p_T, resulting for example from higher-order contributions such as $gu \rightarrow W^+d$ and $u\overline{d} \rightarrow W^+g$, or from primordial p_T of the initial partons.

Usually W production is identified by requiring charged leptons with large p_T and large missing transverse energy, due to the undetected neutrino. Since none of the detectors at RHIC is hermetic, measurement of missing p_T is not available, which leads to some background. Possible sources of leptons with high p_T include charm, bottom, and vector boson production. Above $p_T \geq 20$ GeV/c, leptons from W decay dominate, with a smaller contribution from Z^0 production. Both PHENIX and STAR can estimate the single-lepton Z^0 background from measured Z^0 production. The additional background from misidentified hadrons is expected to be small.

Expected yields were estimated with PYTHIA (108) and RESBOS (109). The cross section at RHIC for W^+ (W^-) production is about 1.3 nb (0.4 nb). These estimates vary by 5–10% according to the choice of the parton distribution set. For 800 pb^{-1} and $p_T \geq 20$ GeV/c, PHENIX expects about 8000 W^+s and 8000 W^-s in the muon arms (that the numbers are equal is due to the decay angle distribution and acceptance), as well as 15,000 W^+ and 2500 W^- electron decays in the central arms. STAR, with its large acceptance for electrons, expects 72,000 W^+s and 21,000 W^-s. Using Equation 20 to reconstruct x, Figure 13 shows the expected sensitivity for $\Delta f(x)/f(x)$, with $f = u, d, \overline{u}, \overline{d}$, for the PHENIX muon data.

RHIC will also significantly contribute to our knowledge about the unpolarized parton densities of the proton, since it will have the highest-energy pp collisions. $\overline{p}p$ production of Ws has a much stronger valence component in the determined (110) $u(x)/d(x)$ ratio. Isospin dependence in Drell-Yan production of muon pairs in pp, pd scattering (97), violation of the Gottfried sum rule (111, 96), and recent semi-inclusive DIS measurements (98) have shown that the unpolarized sea is not $SU(2)$ symmetric. At RHIC, the ratio of unpolarized W^+ and W^- cross sections will directly probe the $\overline{d}/\overline{u}$ ratio, as shown in Figure 14.

4.2 Drell-Yan Production of Lepton Pairs

Drell-Yan production of lepton pairs has been a basis for information about sea quarks (97). At lowest order, lepton pairs are created from quark-antiquark annihilation. With knowledge of the quark densities, Drell-Yan cross sections give the antiquark distributions versus x. The spin asymmetry A_{LL} for Drell-Yan lepton pair production in collisions of longitudinally polarized proton beams is proportional to a sum of contributions over quark flavors, each a product of the polarized

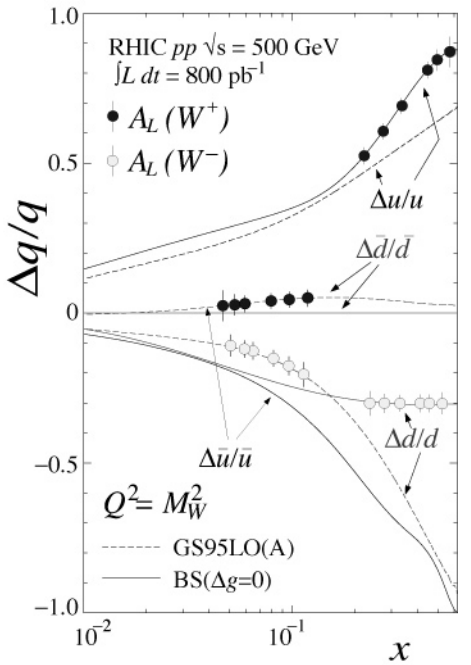

Figure 13 Expected sensitivity for the flavor-decomposed quark and antiquark polarization overlayed on the parton densities of Reference 101 (BS) and of Reference 44 [GS95LO(A)]. Darker points and error bars refer to the sensitivity from $A_L\,(W^+)$ measurements, and lighter ones correspond to $A_L\,(W^-)$.

quark density times the antiquark distribution. The subprocess analyzing power is maximally negative, $\hat{a}_{LL} = -1$. One therefore has, at lowest order,

$$A_{LL} = \hat{a}_{LL} \times \frac{\sum_q e_q^2\{\Delta q(x_1)\Delta\overline{q}(x_2) + \Delta\overline{q}(x_1)\Delta q(x_2)\}}{\sum_q e_q^2\{q(x_1)\overline{q}(x_2) + \overline{q}(x_1)q(x_2)\}}. \qquad 23.$$

This asymmetry is parity-conserving if the process proceeds via a photon. Since the cross sections by flavor are weighted by the electric charge squared, the asymmetry is dominated by the $u\overline{u}$ combination and gives information on the $\overline{u}$ polarization, with the u quark polarization as input. NLO corrections to the asymmetry have been calculated (106, 102) to be small for low p_T of the virtual photon. For higher p_T, Drell-Yan production is sensitive to $\Delta g(x)$ through $qg \rightarrow \gamma^* q$ (37, 72, 73), as discussed in Section 3.

However, lepton pair production in high-energy pp collisions is dominated by coincidental semileptonic decays of heavy-quark pairs, e.g. $b \rightarrow c\,l^-\,\overline{\nu}$ in the low-mass region. The feasibility of the measurements will therefore depend on the ability to separate or estimate this background. Estimates of the yields in the PHENIX muon arms obtained with PYTHIA for pp collisions at $\sqrt{s} = 200$ GeV show that lepton pairs with invariant mass $M \geq 6\ \mathrm{GeV}/c^2$ are dominated by Drell-Yan production. One expects ∼40,000 pairs for a nominal integrated luminosity of 320 pb^{-1}.

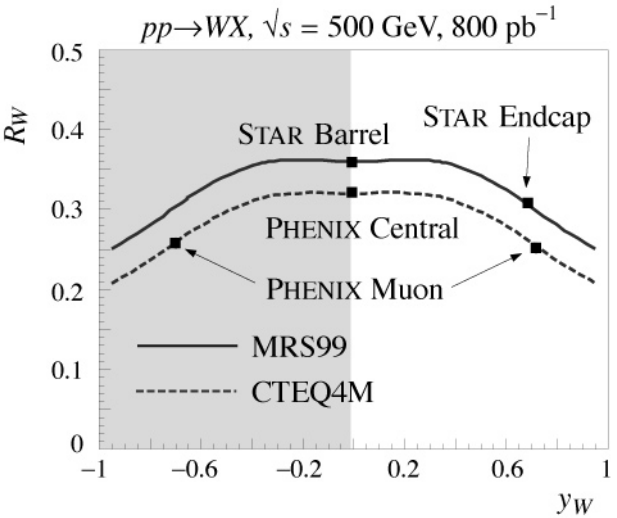

Figure 14 The ratio $R_W = (d\sigma(W^-)/dy)/(d\sigma(W^+)/dy)$ for unpolarized pp collisions at RHIC. The shaded region indicates that unpolarized pp collisions are symmetric in y_W. To illustrate the sensitivity of the measurement, we show an earlier set of parton densities [CTEQ4M (112)] and a set [MRS99 (113)] that includes the latest information from Drell-Yan data (97). Both curves include an asymmetric sea with $\bar{d}/\bar{u}$ rising to 1.6 for increasing antiquark momentum fraction $x_{\bar{q}}$, but the latter also includes a drop-off in the ratio for higher $x_{\bar{q}}$.

5. TRANSVERSE AND FINAL-STATE SPIN EFFECTS

Exciting physics prospects also arise for transverse polarization of the RHIC proton beams. One is the possibility of a first measurement of the quark transversity densities introduced in Table 1. The transversity distributions, measuring differences of probabilities for finding quarks with transverse spin aligned and anti-aligned with the transverse nucleon spin, are as fundamental as the longitudinally polarized densities for quarks and gluons, Δq, Δg; they have evaded measurement so far because they decouple from inclusive DIS. Comparisons of the polarized quark distributions δq and Δq are particularly interesting; in the nonrelativistic limit, where boosts and rotations commute, one has $\delta q(x, Q^2) = \Delta q(x, Q^2)$. Deviations from this provide a measure of the relativistic nature of quarks inside the nucleon.

Studies of single-transverse spin asymmetries, defined similarly to Equation 10, will be a further interesting application. They arise as "higher-twist" effects (that is, they are suppressed by inverse powers of the hard scale) and probe quark-gluon correlations in the nucleon. They have an exciting history in experiments that were carried out at energies much lower than RHIC's, where large polarizations and single-spin asymmetries have been seen (114). Yet another field of spin physics

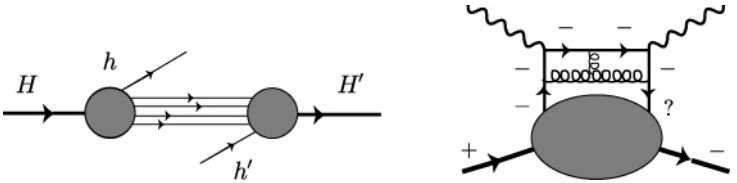

Figure 15 *Left:* quark densities as related to polarized quark-hadron forward scattering in the u-channel. Labels refer to helicities. *Right:* decoupling of transversity from deep-inelastic scattering (116). Quark chirality is not changed by coupling to a photon or a gluon.

to be thoroughly examined by the RHIC experiments will be the transfer of longitudinal or transverse polarization from the initial into the final state, which then leaves traces in the polarization of hadrons produced in the fragmentation process.

5.1 The Quark Transversity Distributions

The transversity densities δq and $\delta\overline{q}$ are virtually inaccessible in inclusive DIS (11, 17). We can see this as follows (115). In a simple parton model, and working in a helicity basis, we can view the quark densities as imaginary parts of polarized quark-hadron forward scattering in the u-channel, denoted by $\mathcal{A}(H, h; H', h')$ (see Figure 15). One then has $q = \mathcal{A}(++; ++) + \mathcal{A}(+-; +-)$, $\Delta q = \mathcal{A}(++; ++) - \mathcal{A}(+-; +-)$, but $\delta q = \mathcal{A}(++; --)$. Thus, for transversity to contribute, the quark has to undergo a helicity flip in the hard scattering, which is not allowed (for massless quarks) at the DIS quark-photon vertex due to helicity conservation. Note the striking feature that the helicity labels of the final state in $\mathcal{A}(++; --)$ differ from those of the initial state. In other words, the complex conjugate amplitude contained in $\mathcal{A}(++; --)$ refers to a different physical state than the initial. This "off-diagonal" nature in terms of helicity is usually referred to as chiral-odd (11) and can indeed in practice only be achieved by having transverse polarization, which can be written as a superposition of helicity states.

Another important consequence is that, unlike the situation for unpolarized and longitudinally polarized densities, there is no transversity gluon distribution (11, 16, 17). This is due to angular momentum conservation; a gluonic helicity-flip amplitude would require the hadron to absorb two units of helicity, which a spin-1/2 target cannot do.

The joint description of the quark distributions in terms of the $\mathcal{A}(H, h; H', h')$ implies that transversity is not entirely unrelated to the $q, \Delta q$. Indeed, rewriting (115) $\mathcal{A}(H, h; H', h') = \sum_X a^*_{H'h'}(X) a_{Hh}(X)$, where X is an arbitrary final state, one finds from the condition $\sum_X |a_{++}(X) \pm a_{--}(X)|^2 \geq 0$ the inequality (117)

$$q(x) + \Delta q(x) \geq 2|\delta q(x)| \ . \qquad 24.$$

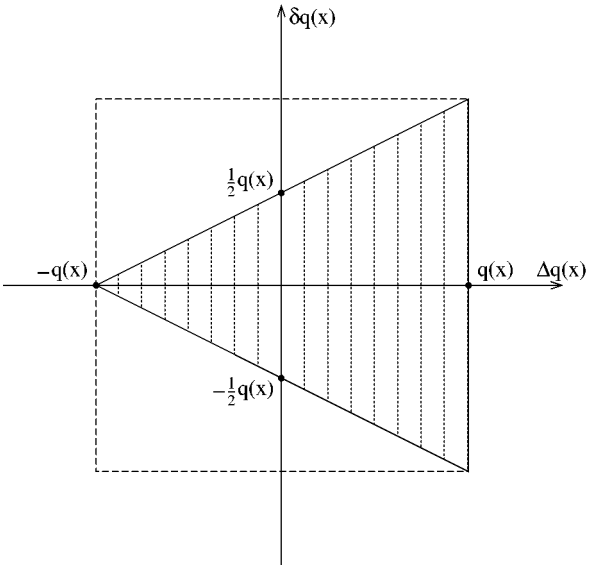

Figure 16 The hatched area represents the domain allowed by positivity, Equation 24.

Figure 16 displays the region allowed by Equation 24, which is indeed smaller than the one resulting from the trivial condition $|\delta q(x)| \leq q(x)$. Equation 24 holds for all quark flavors and separately for their corresponding antiquarks. As was demonstrated (118–121), the inequality is preserved under QCD evolution; that is, if it is assumed to be satisfied at one resolution scale, it will hold at all larger scales. This remains true (119–121) even at two-loop order (119, 122) in evolution.

The helicity flip required for transversity to contribute to hard scattering can occur if there are two soft hadronic vertices in the process. In this case, transverse spin can be carried from one hadron to the other along a quark line. One possibility is to have two transversely polarized hadrons in the initial state, as realized at RHIC. An alternative is to have one transversely polarized initial hadron and a final-state fragmentation process that is sensitive to transverse polarization. Here, the other initial particle could be a lepton, as in DIS, or another proton, as at RHIC.

For the first possibility, a promising candidate process for a measurement of the δq, $\delta\overline{q}$ is Drell-Yan dimuon production which, to lowest order in QCD, proceeds via $q\overline{q} \to \gamma^*$ annihilation. A systematic study of this process was in fact also the place where the transversity densities made their first appearance in theory (15). The downside of this reaction is that the transversity antiquark density in the nucleon is presumably rather small; there is no splitting term $g \to q\overline{q}$ in the evolution equations for transversity (17), so a vital source for the generation of antiquarks is missing [only higher orders in evolution produce antiquarks carrying transversity (119, 121)]. Also, in Drell-Yan, the event rate is generally low. However, when

compared to other conceivable reactions in pp collisions that serve to determine parton densities, the Drell-Yan process has the advantage that to lowest order there is no partonic subprocess that involves a gluon in the initial state. If a reaction does have a gluon-initiated subprocess, its transverse double-spin asymmetry is expected to be suppressed (123, 20). This is because gluons usually strongly contribute to the unpolarized cross sections in the denominator of the asymmetry, whereas they are absent for transversity, as discussed above. In addition, for many reactions other than Drell-Yan, one finds a particular "selection-rule" (123, 20) suppression of the contributing transverse subprocess asymmetries.

Several phenomenological studies of Drell-Yan dimuon production at RHIC have been presented (124, 125, 101, 126, 121, 127). Model estimates of the transversity densities have been obtained in these studies by either assuming $2\delta q(x, Q_0^2) = q(x, Q_0^2) + \Delta q(x, Q_0^2)$ (see Equation 24), or by employing (127, 128) $\delta q(x, Q_0^2) \simeq \Delta q(x, Q_0^2)$, at some initial (low) resolution scale Q_0. Note that the latter ansatz violates inequality 24 if $\Delta q(x, Q_0^2) < -\frac{1}{3} q(x, Q_0^2)$. The transverse double-spin asymmetry for Drell-Yan dimuon production is (to lowest order)

$$A_{TT} = \widehat{a}_{TT} \frac{\sum_q e_q^2 \delta q(x_1, M^2) \delta \overline{q}(x_2, M^2) + (1 \leftrightarrow 2)}{\sum_q e_q^2 q(x_1, M^2) \overline{q}(x_2, M^2) + (1 \leftrightarrow 2)}. \qquad 25.$$

Here $\widehat{a}_{TT}$ is the partonic transverse-spin asymmetry, calculable in perturbative QCD, and M is the dilepton mass. NLO corrections to Drell-Yan dimuon production with transversely polarized beams have been calculated (124, 125, 121, 129, 130) and are routinely used in numerical studies.

The PHENIX endcaps will be able to identify muons with rapidity $1.2 < |y_{\mu^\pm}| < 2.4$. Figure 17 shows predictions (121) for A_{TT}. In order to model the transversity densities, saturation of inequality 24 at a low scale $Q \approx 0.6$ GeV has been assumed, making use of the information on the Δq, $\Delta \overline{q}$ in that inequality coming from polarized DIS. The statistical errors expected for PHENIX are also shown. One observes that the asymmetry is generally small but could be visible experimentally

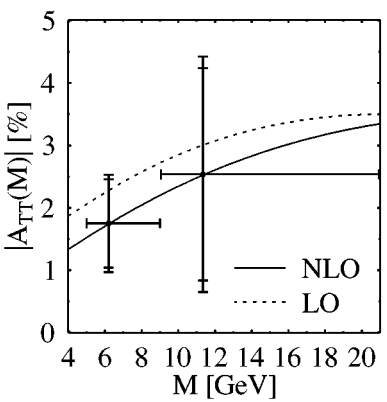

Figure 17 Next-to-leading-order transverse-spin asymmetry for Drell-Yan dimuon production at $\sqrt{s} = 200$ GeV (121).

if the transversity densities are not much smaller than those used here. Larger estimates for A_{TT} have been obtained (101), based on more optimistic assumptions concerning the size of the δq, $\delta\overline{q}$. Careful studies of the background to lepton pair production resulting from coincidental semileptonic heavy-flavor decays (see Section 4) will be important.

The other possibility involves one transversely polarized initial hadron and a final-state fragmentation process that is sensitive to transverse polarization. Promising approaches have emerged from considering the production of high-p_T dimeson systems (131, 12, 132), or from taking into account "intrinsic" transverse momentum degrees of freedom in a fragmentation process producing a single high-p_T pion 133). Both dimesons and pions are very abundantly produced in high-energy pp collisions. It has been shown (131) that the azimuthal distribution of low-mass pairs of pions about the final-state jet axis can be used as a measure of the transverse polarization of the quark initiating the jet. The same is true (133) for the "intrinsic" transverse momentum distribution of a produced pion relative to its quark progenitor. In this way, one effectively obtains an asymmetry that is sensitive to products of the transversity density for the initial-state quark and a transverse-polarization–dependent fragmentation function for the final state. For instance, for the mechanism proposed for DIS in Reference 133, the fragmentation function would be

$$H_1^{\perp}(z, k_{\perp}) \propto D_{\pi/q\uparrow}(z, k_{\perp}) - D_{\pi/q\downarrow}(z, k_{\perp}), \qquad 26.$$

where $k_{\perp}$ is the "intrinsic" transverse momentum in the fragmentation process. Notice that one polarized proton in the initial state is sufficient for this kind of measurement. Time-reversal invariance, however, precludes a nonzero effect unless phases are generated by final-state interactions in the fragmentation process that do not average to zero upon summation over unobserved hadrons. It is a priori unclear whether such a net phase will exist. This led to investigation (132) of the interference between s and p waves of two-pion systems with invariant mass around the ρ. Such an interference effect yields sensitivity to the polarization of the quark progenitor through the quantity $\vec{k}_{\pi^+} \times \vec{k}_{\pi^-} \cdot \vec{s}_T$, where the $\vec{k}$s are the pion momenta and $\vec{s}_T$ is the transverse nucleon spin; one effectively uses the angular momentum of the two-pion system as a probe of the quark's polarization. Staying in the mass region around the ρ ensures (132) that the final-state interaction phase does not average to zero. The s-p wave interference in the $q \to \pi\pi$ formation is described by a new set of fragmentation functions, the interference fragmentation functions (132). Just as the function in Equation 26, the latter are presently entirely unknown; the price to be paid for obtaining sensitivity to transversity in all of the ways suggested in References 131, 132, and 133 is thus the introduction of another unknown component. However, one may hope that the involved fragmentation functions can be determined independently in e^+e^- annihilation. Studies of the experimental situation at RHIC concerning the proposal of Reference 132 are under way (134).

5.2 Transverse Single-Spin Asymmetries

Surprisingly large single-transverse spin asymmetries, for instance in fixed-target $p^{\uparrow} p \to \pi X$ at pion transverse momenta of a few GeV, have been observed experimentally (114) over many years. RHIC will further investigate the origin of such asymmetries. Within the "normal" framework of perturbative QCD and the factorization theorem at twist-2 for collinear massless parton configurations, no single-transverse spin asymmetry is obtained—nonzero effects occur only when one keeps quark mass terms (as is required to generate helicity flips) and when one takes into account at the same time higher-order loop diagrams that produce relative phases (18). Such effects are therefore of the order of $\alpha_s m_q/\sqrt{s}$ and cannot explain data such as that in Reference 114. It is believed that nontrivial higher-twist effects are responsible for the observed single-spin asymmetries (135, 136, 138). References 136 and 138 showed how single transverse-spin asymmetries can be evaluated consistently in terms of a generalized factorization theorem in perturbative QCD, wherein they arise, for example, as convolutions of hard-scattering functions with an ordinary twist-2 parton density from the unpolarized hadron and a twist-3 quark-gluon correlation function representing the polarized hadron. Another contribution involves the transversity distribution and another (chiral-odd) spin-independent twist-3 function of the proton (138, 139). A simple model was constructed (136, 138) that assumes only correlations of valence quarks and soft gluons. It can describe the present data and makes various definite predictions, to be tested at RHIC, where one certainly expects to be in the perturbative domain. In particular, at RHIC, one should see the fall-off with p_T of the single-transverse spin asymmetries in single-inclusive pion production, associated with their twist-3 nature (see Figure 18).

A related dynamical origin for transverse single-spin asymmetries was proposed (19, 133, 140) to reside in the dependences of parton distribution and fragmentation functions on intrinsic parton transverse momentum k_T. In fact, the proposal of (133) for measuring transversity in the proton, which we discussed in the previous subsection, proceeds for pp scattering exactly through a single-transverse spin asymmetry, making use of the k_T-dependent fragmentation function in Equation 26. Suppression of the asymmetry should also arise here, through a factor $\langle k_T \rangle / p_T$. It has also been considered that single-spin asymmetries might be generated by k_T dependences of the parton distribution functions in the initial state (19, 140). Here, one could have

$$\begin{aligned} f_{1T}^{\perp}(x, k_{\perp}) &= f_{q/p\uparrow}(x, k_{\perp}) - f_{q/p\downarrow}(x, k_{\perp}), \\ h_1^{\perp}(x, k_{\perp}) &= f_{q\uparrow/p}(x, k_{\perp}) - f_{q\downarrow/p}(x, k_{\perp}) \end{aligned} \qquad 27.$$

as the driving forces. There is a qualitative difference between the functions in Equations 27 and 26: In order to be able to produce an effect, the latter requires final-state interactions (which are certainly present), to make the overall process time-reversal-symmetry-conserving (see the previous subsection). In contrast, the

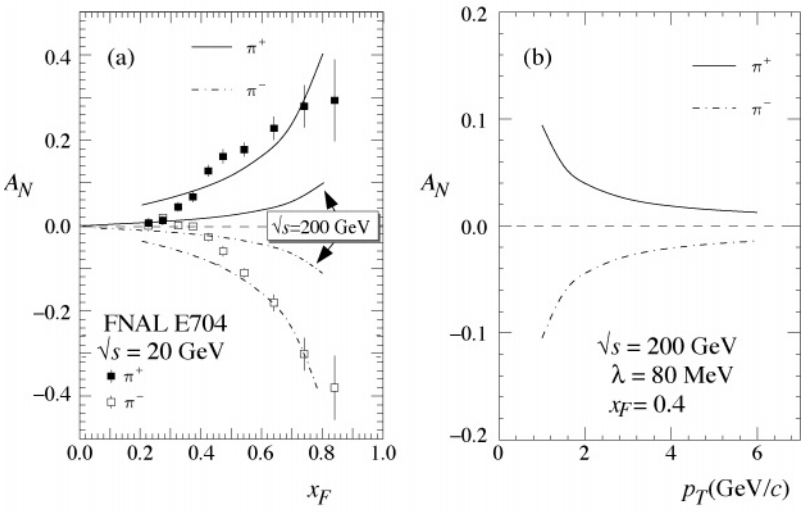

Figure 18 (*a*) Experimental data (137) and theoretical calculations (138) for transverse single-spin asymmetries for π^+ and π^- production in pp collisions at $\sqrt{s} = 20$ GeV as functions of x_F. Predictions for RHIC for $p_T = 4\,\text{GeV}/c$ are superimposed. The transverse momentum dependence for RHIC at $x_F = 0.4$ is shown in (*b*).

distributions in Equation 27 rely on the presence of nontrivial (factorization-breaking) initial-state interactions between the incoming hadrons (141), or on finite-size effects for the hadrons (142); they vanish if the initial hadrons are described by plane waves. This makes the "Collins function" (Equation 26) perhaps a more likely source for single-spin asymmetries. The reservations concerning Equation 27 notwithstanding, when a factorized hard-scattering model is evoked, each mechanism described by Equations 26 and 27 can by itself account for (141, 140, 143) the present $p\uparrow p \to \pi X$ data. Also, all could be at work simultaneously and compete with one another. Single-spin Drell-Yan measurements at RHIC should be a good testing ground (140) for the existence of effects related to Equation 27, since for Drell-Yan the Collins function (Equation 26) cannot contribute.

5.3 Spin-Dependent Fragmentation Functions

Even in the context of a parity-conserving theory like QCD, an asymmetry can arise for only one longitudinally polarized particle in the initial state, if the longitudinal polarization of a particle in the final state is observed. The measurement of the polarization of an outgoing highly energetic particle certainly provides a challenge to experiment. Λ baryons are particularly suited for such studies, thanks to the self-analyzing properties of their dominant weak decay, $\Lambda \to p\pi^-$. Recent results

on Λ production reported from LEP (144) have demonstrated the feasibility of successfully reconstructing the Λ polarization.

Spin-transfer asymmetries give information on yet unexplored spin effects in the fragmentation process. For our Λ example, the longitudinal transfer asymmetry will be sensitive to the functions

$$\Delta D_i^{\Lambda}(z) \equiv D_{i(+)}^{\Lambda(+)}(z) - D_{i(+)}^{\Lambda(-)}(z) \qquad 28.$$

describing the fragmentation of a longitudinally polarized parton $i = q, \overline{q}, g$ into a longitudinally polarized Λ, where $D_{i(+)}^{\Lambda(+)}(z)[D_{i(+)}^{\Lambda(-)}(z)]$ is the probability of finding a Λ with positive (negative) helicity in a parton i with positive helicity, carrying a fraction z of the parent parton's momentum (see Section 2). As was shown (145, 146), the LEP measurements (144) have provided initial information on some combinations of the ΔD_i^{Λ} but leave room for very different pictures of the spin-dependence in Λ fragmentation. Measurements of the polarization of Λs produced in $\vec{p}p$ collisions at RHIC should vastly improve (147, 148) our knowledge of the ΔD_i^{Λ}. Figure 19 illustrates this by showing the longitudinal spin transfer asymmetry at RHIC, defined in analogy with Equation 7 as

$$A^{\Lambda} = \frac{\left(\sigma_+^{\Lambda(+)} + \sigma_-^{\Lambda(-)}\right) - \left(\sigma_-^{\Lambda(+)} + \sigma_+^{\Lambda(-)}\right)}{\left(\sigma_+^{\Lambda(+)} + \sigma_-^{\Lambda(-)}\right) + \left(\sigma_-^{\Lambda(+)} + \sigma_+^{\Lambda(-)}\right)}, \qquad 29.$$

where the lower helicity index refers to the polarized proton and the upper to the produced Λ. Various models for the ΔD_i^{Λ}, all compatible with the LEP data, have

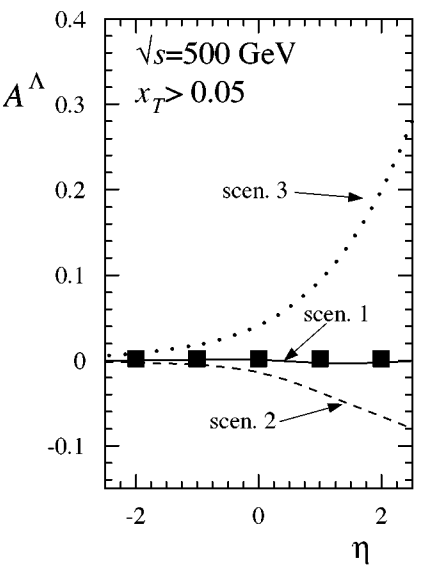

Figure 19 The longitudinal spin transfer asymmetry in Λ production at RHIC ($\sqrt{s} =$ 500 GeV) (147), as a function of rapidity of the Λ for various sets of spin-dependent fragmentation functions proposed in Reference 145. For scenario 1, only strange quarks transmit polarization to the Λ. In scenario 2, there is also a (negative) contribution from up and down quarks (149). In scenario 3, all quarks equally produce polarized Λs. The expected errors for STAR with standard luminosity and polarization are comparable to the "data" shown for $\eta = \pm 2$, and smaller for the other points.

been used in Figure 19. It will be interesting to see which scenario is favored by the RHIC measurements. A cut of $x_T > 0.05$ has been applied in the figure. Λs are very copiously produced at RHIC (147), resulting in small expected statistical errors.

Similarly optimistic conclusions have been reached (150) for the case of transverse polarization of one initial beam and the Λ, in which case RHIC experiments would yield information on the product of the proton's transversity densities and the transversity fragmentation functions of the Λ, which so far are both unknown.

6. PHYSICS BEYOND THE STANDARD MODEL

So far we have discussed probing the proton spin structure at RHIC, and both using and testing perturbative QCD in the spin sector. Spin is also an excellent tool to go beyond the standard model and to uncover important new physics, if it exists. Many extensions of the standard model have been proposed. Our purpose in this section is to illustrate this new potentiality by means of a specific example.

Let us consider one-jet inclusive production. As discussed in Section 3, the cross section is dominated by the pure QCD gg, gq, and qq scatterings, but the existence of the electroweak interaction, via the effects of the $W^{\pm}$ and Z gauge bosons, adds a small contribution. Consequently, the parity-violating helicity asymmetry A_L, defined as (151)

$$A_L = \left[\frac{d\sigma_-^{pp\to jetX}}{dE_T} - \frac{d\sigma_+^{pp\to jetX}}{dE_T}\right] \cdot \left[\frac{d\sigma_+^{pp\to jetX}}{dE_T} + \frac{d\sigma_-^{pp\to jetX}}{dE_T}\right]^{-1}, \qquad 30.$$

is expected to be nonzero from the QCD-electroweak interference (as shown in Figure 20). Additionally, a small peak near $E_T = M_{W,Z}/2$ is seen, which is the main signature of the purely electroweak contribution. The cross sections are for one longitudinally polarized beam colliding with an unpolarized beam. The existence of new parity-violating interactions could lead to large modifications of this standard-model prediction (151).

First let us recall that the sensitivity to the presence of some new quark-quark contact interaction has been analyzed (152). Such a contact interaction could represent the effects of quark compositeness, under the form

$$\mathcal{L}_{qqqq} = \epsilon \frac{g^2}{8\Lambda^2} \overline{\Psi}\gamma_\mu(1-\eta\gamma_5)\Psi \cdot \overline{\Psi}\gamma^\mu(1-\eta\gamma_5)\Psi, \qquad 31.$$

where Ψ is a quark doublet, Λ is a compositeness scale, and $\epsilon = \pm 1$. If parity is maximally violated, $\eta = \pm 1$. Figure 20 shows how the standard-model prediction will be affected by such a new interaction, assuming $\Lambda = 2$ TeV, which is close to the present limit obtained for example by the DØ experiment at the Tevatron (153). The statistical errors shown are for standard RHIC luminosity of 800 pb^{-1}, and for jets with rapidity $|y| < 0.5$, and include measuring A_L using each beam, summing over the spin states of the other beam. Due to the parity-violating signal's

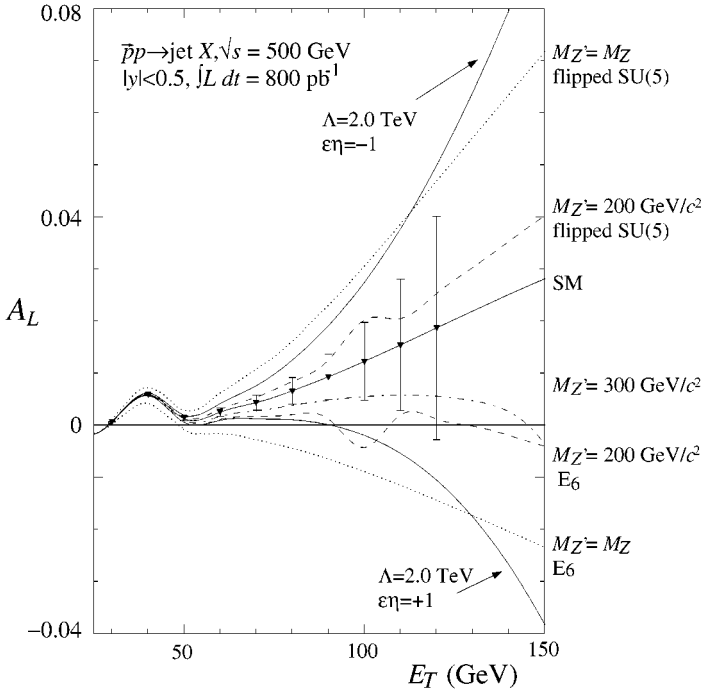

Figure 20 A_L for one-jet inclusive production in $\vec{p}\,p$ collisions, versus transverse energy, for $\sqrt{s} = 500$ GeV. The solid curve with error bars represents the standard-model expectation. The error bars show the sensitivity at RHIC for 800 pb^{-1}, for the STAR detector. The other solid curves, labeled by the product of $\epsilon\eta$, correspond to the contact interaction at $\Lambda = 2$ TeV (152). The dashed and dotted curves correspond to different leptophobic Z' models (154). The calculations are at leading order.

sensitivity to new physics, RHIC is surprisingly sensitive to quark substructure at the 2-TeV scale and is competitive with the Tevatron, despite the different energy ranges of these machines. Indeed, a parity-violating signal beyond the standard model at RHIC would definitively indicate the presence of new physics (151).

RHIC-Spin would also be sensitive to possible new neutral gauge bosons (154). A class of models, called leptophobic Z', is poorly constrained up to now. Such models appear naturally in several string-derived models (155) [nonsupersymmetric models may be also constructed (156)]. In addition, in the framework of supersymmetric models with an additional Abelian gauge factor $U(1)'$, it has been shown (157) that the Z' boson could appear with a relatively low mass ($M_Z \leq M_{Z'} \leq 1$ TeV) and a mixing angle with the standard Z close to zero. The effects of different representative models are shown in Figure 20 (see Reference 154 for details). RHIC covers some regions in the parameter space of the different models that are unconstrained by present and forthcoming experiments (e.g. Tevatron

Run II), and RHIC would also uniquely obtain information on the chiral structure of the new interaction.

Other possible signatures of new physics at RHIC have been investigated. Particularly interesting quantities (100, 158, 159) are transverse (single or double) spin asymmetries for $W^{\pm}$ production, since these are expected to be extremely small in the standard model (100, 160). For instance, the case of the corresponding standard-model double spin asymmetry $A_{TT}^{\pm}$ was examined in detail recently (160). Non-vanishing contributions could arise here for example in the form of higher-twist terms, which would be suppressed as powers of M^2/M_W^2, where M is a hadronic mass scale and M_W the W mass. Other possible contributions were demonstrated (160) to be negligible as well. By similar arguments, also the corresponding single-transverse spin asymmetry for $W^{\pm}$ production, $A_N^{\pm}$, is expected to be extremely small in the standard model (159). New physics effects, on the contrary, might generate asymmetries at leading twist, for example through non-$(V-A)$ (axial)vector couplings of quarks to the W, or through tensor or (pseudo)scalar couplings, all of which would also have to violate CP in order to generate a single-spin asymmetry $A_N^{\pm}$. In particular the latter asymmetry has been examined with respect to sensitivity to new physics effects at RHIC (159). For a case study, the minimal supersymmetric extension of the standard model, with R-parity violation, was employed, which contains scalar quark-W interactions and complex phases, resulting in CP-violating effects. The results of Reference 159 show that in this particular extension of the standard model, $A_N^{\pm}$ is likely to be very small as well, below the detection limit of RHIC. Nevertheless, this does not exclude the possibility that other non-standard mechanisms produce larger effects, and $A_N^{\pm}$ and $A_{TT}^{\pm}$ will be measured at RHIC with transversely polarized beams in the context of the physics discussed in the previous section. A non-zero result would be a direct indication of new physics.

7. SMALL-ANGLE *pp* ELASTIC SCATTERING

In previous sections, we have discussed the physics of hard scattering at RHIC with polarized protons, which can be understood as collisions of polarized quarks and gluons. The scattering is so energetic that we can use perturbative QCD to describe the interactions of the quarks and gluons and, thus, probe the spin structure of the proton at very small distances. For example, scattering at $Q^2 = (80\ \mathrm{GeV})^2$ probes wave lengths of 0.003 fermi. Small-angle scattering, from total cross section to $t = -1\ (\mathrm{GeV}/c)^2$, probes the static proton properties and constituent quark structure of the proton, covering distances from 4 fermi [$-t = 0.003\ (\mathrm{GeV}/c)^2$ in the Coulomb nuclear interference (CNI) region] to a distance of $\approx$0.2 fermi. Unpolarized scattering shows striking behavior in this region, from the surprise that total cross sections rise at high energy, to observed dips in elastic cross sections around $-t = 1\ (\mathrm{GeV}/c)^2$. The PP2PP experiment at RHIC (29) will explore this region for spin-dependent cross sections, for $\sqrt{s} = 20-500$ GeV, for the first time.

Historically, new spin-dependent data have often shown new structure underlying spin-independent cross sections, indicating the presence of unexpected dynamics in the interaction. Several examples have been discussed in previous sections. Previous work with spin stops at $\sqrt{s} = 20$ GeV, where tertiary polarized p and $\overline{p}$ beams were collected from the parity-violating decays of Λ and $\overline{\Lambda}$ hyperons and steered onto unpolarized hydrogen and polarized pentanol ($C_5H_{12}O$) targets (161). RHIC will provide much higher intensity, a large extension of the energy range, and pure targets for 2-spin measurements.

In the energy regime $\sqrt{s} > 20$ GeV, total cross sections have been observed to rise with energy for $pp, \overline{p}p, \pi^{\pm}p$, and $K^{\pm}p$. The $\overline{p}p$ total cross section rises through the Tevatron maximum energy of 2 TeV, and the pp total cross section has been observed to rise through its highest energy measurement at the ISR, $\sqrt{s} = 62$ GeV (162). The PP2PP experiment will measure spin-dependent total cross sections, $\sigma_{\uparrow\uparrow}$, $\sigma_{\uparrow\downarrow}$, and $\sigma_L = \sigma_+ - \sigma_-$ [where the arrows represent transverse spin measurements, and $(+)$ and $(-)$ represent helicities] through the range of rising cross sections available at RHIC. The unpolarized pp total cross section measurements will also be extended to $\sqrt{s} = 500$ GeV.

For $\overline{p}p$, the rise of the total cross section has been successfully described in the impact picture approach on the basis of the high-energy behavior of a relativistic quantum field theory (163). This is based on the fact that the effective interaction strength increases with energy in the form $s^{1+c}/(ln\ s)^{c'}$, a simple expression in two key parameters c and c', where s is expressed in GeV^2. A fit of the data then leads to the values of the two free parameters $c = 0.167, c' = 0.748$ (164). If this picture is correct (the field theoretical argument is based on connecting QED and QCD theories, but it successfully predicted that the $\overline{p}p$ total cross section would continue to rise, following these parameters), there should be no difference in the rise of pp and $\overline{p}p$ total cross sections. An extension of this approach allows a description of the elastic cross section (165), which will also be measured at RHIC.

The single-spin asymmetry for pp elastic scattering, A_N, is expected to be small but significant in the CNI region, $-t = 0.001$–0.01 $(\text{GeV}/c)^2$ (166). As discussed previously, pp elastic scattering in the CNI region will be the basis of the RHIC polarimetry. CNI scattering is expected to produce an asymmetry from scattering an unpolarized proton (polarization averaged to zero) in one beam from the magnetic moment of a polarized proton from the other beam, with a maximum of $A_N = 0.04$ at $-t = 0.003$ $(\text{GeV}/c)^2$. However, a hadronic spin-flip term can also contribute to the maximum, and this term is sensitive to the static constituent quark structure of the proton. Buttimore et al (166) remark that the helicity flip probes the shortest interquark distance in the proton, and that the helicity nonflip is sensitive to the largest quark separation in the proton due to color screening. The helicity-flip term, if present, can indicate an isoscalar anomalous magnetic moment of the nucleons (167), an anomalous color-magnetic moment causing helicity nonconservation at the constituent quark-gluon vertex (168), and/or a compact quark pair in the proton (24, 169).

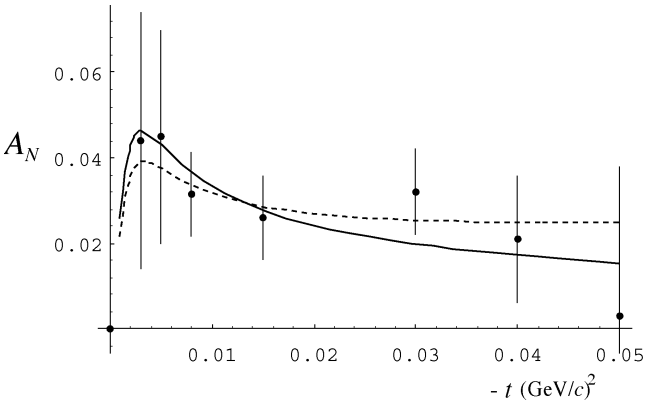

Figure 21 Transverse single-spin asymmetry for proton proton elastic scattering. The data points are from Fermilab E704 (161). The solid curve is the best fit with the spin-flip hadronic amplitude constrained to be in phase with non-flip hadronic amplitude; the dotted curve is the best fit without this constraint.

The only measurement of A_N in the CNI region at higher energy is by E704 at Fermilab (161) at a lab momentum $p_L = 200$ GeV/c; the results are shown in Figure 21. The errors are too large to allow an unambiguous theoretical interpretation. There are two fits to the E704 data shown with a nonzero hadronic spin flip term (25). As emphasized in References 25 and 26, a large value of the hadronic helicity-flip amplitude generates a very large change in the maximum in A_N, which can be of the order of 30% or more. The PP2PP experiment will measure A_N to ± 0.001 in the CNI peak. This level of precision is required for absolute polarimetry, giving an expected precision on A_N of $\Delta A_N/A_N = \pm 0.001/0.04 = \pm 0.025$. This experiment will cover from $0.0005 \leq -t \leq 1.5$ (GeV/c)^2 (with additional detectors for the larger $-t$ region). Thus, the location of the maximum in A_N and its maximum value and shape will be determined.

Small-angle scattering at high energy is presently understood in the Regge picture as being dominated by Pomeron exchange (170). The Pomeron, which has the vacuum quantum numbers with charge-conjugation $C = +1$, can be interpreted as a two-gluon exchange. There is room in the data for a small three-gluon exchange contribution with $C = -1$, the Odderon (171). It has been shown recently (172) that the behavior of the two-spin transverse asymmetry A_{NN} in pp elastic scattering in the CNI region depends strongly on the Odderon contribution and that the PP2PP experiment is quite sensitive to its presence.

In addition to the measurements discussed above, the PP2PP experiment will measure larger angles, to $-t = 1.5$ (GeV/c)^2, which includes the region of dip structure in the unpolarized cross section, measuring A_N and the two-spin asymmetries A_{NN}, A_{SS}, and A_{LL} (166). These first, precise, determinations of spin dependence for small-angle pp elastic scattering in the energy range

$\sqrt{s}$ = 20–500 GeV probe the spin structure of the proton in the nonperturbative QCD region, from the static properties of the proton to its constituent quark structure.

At higher energy, such as at the LHC, the CNI region becomes inaccessible. The minimum $-t$ reachable with colliding beams depends on scattering the protons out of the beams. For fixed $-t$, the scattering angle falls as $1/p_{beam}$, whereas the beam size falls more slowly as $1/\sqrt{p_{beam}}$. Roughly, this limits an experiment at the LHC to $-t > 0.01$ (GeV/c)^2.

8. CONCLUDING REMARKS

RHIC will be the first machine to look at the proton spin structure by colliding polarized proton beams rather than scattering polarized leptons off polarized targets. Thus, one can test fundamental interactions in an entirely different environment and at much higher energies, as in the unpolarized case. (Here, too, information on the nucleon structure from DIS has been complemented by information from hadron colliders.) For hadron colliders, including RHIC-Spin, due to the high energy and luminosity that give access to hard parton scattering, perturbative QCD probes in one proton are used to study the nonperturbative structure of the "target" proton.

What can we expect from RHIC-Spin? If, for example, a large gluon polarization is observed, such a signal would imply a previously unknown fundamental role of the gluons in the proton spin. Surprise and new insights are very likely.

This field is very new both theoretically and experimentally. Previous experimental spin work with hadron probes was at much lower energy and luminosity, and used impure polarized targets. Much of the discussion presented here is from very recent work. Thus, this article should not be seen as a review but rather as an invitation.

ACKNOWLEDGMENTS

This article summarizes the hard work of many collaborators in theoretical, experimental, and accelerator physics who have developed the RHIC spin program. Leaders in this program from its beginnings to the present include Michael Tannenbaum, Yousef Makdisi, and Thomas Roser of Brookhaven; the Marseille Theory Group; and Aki Yokosawa, Hal Spinka, and Dave Underwood of Argonne. The Kyoto, Penn State, UCLA, and IHEP groups have contributed many ideas and studies, including Vladimir Rykov of Wayne State University (previously of IHEP). Robert Jaffe of MIT helped initiate a close collaboration between theorists and experimenters to develop the RHIC spin program. We acknowledge important ideas and work by Leslie Bland and colleagues at Indiana University. In addition, we would like to thank Daniel Boer, Akira Masaike, Marco Stratmann, Lawrence Trueman, Jean-Marc Virey. The key step in this spin program, leading to its anticipated first run in 2001, has been the involvement of RIKEN,

Japan. RIKEN has supported, beginning in 1995, the spin hardware, including the Siberian Snakes and Spin Rotators, and a second muon arm for spin for PHENIX; it created the RIKEN BNL Research Center to develop our understanding of RHIC physics, and it supports a strong spin group based at Brookhaven. The Science and Technology Agency of Japan supports RIKEN. We thank the US Department of Energy for its early support of the RHIC spin program.

APPENDIX: Information from Polarized Deep-Inelastic Scattering

In this Appendix we briefly discuss the information from DIS on Δq, $\Delta\overline{q}$, Δg. If we neglect contributions resulting from $W^{\pm}$ or Z^0 exchange, DIS is sensitive only to the sums of quarks and antiquarks for each flavor. Therefore, we define

$$\Delta\mathcal{Q}(x, Q^2) \equiv \Delta q(x, Q^2) + \Delta\overline{q}(x, Q^2). \tag{32.}$$

To lowest order, we can then write the structure functions g_1^p, g_1^n appearing in DIS off polarized proton and neutron targets as

$$\begin{aligned} 2g_1^p(x, Q^2) &= \frac{4}{9}\Delta\mathcal{U}(x, Q^2) + \frac{1}{9}[\Delta\mathcal{D}(x, Q^2) + \Delta\mathcal{S}(x, Q^2)]\,, \\ 2g_1^n(x, Q^2) &= \frac{4}{9}\Delta\mathcal{D}(x, Q^2) + \frac{1}{9}[\Delta\mathcal{U}(x, Q^2) + \Delta\mathcal{S}(x, Q^2)]\,, \end{aligned} \tag{33.}$$

where all parton densities refer to the proton. We can compactly rewrite this as

$$g_1^{p,n}(x, Q^2) = \pm\frac{1}{12}\Delta\mathcal{A}_3(x, Q^2) + \frac{1}{36}\Delta\mathcal{A}_8(x, Q^2) + \frac{1}{9}\Delta\Sigma(x, Q^2)\,, \tag{34.}$$

where the upper sign refers to the proton, and where we have introduced the flavor–non-singlet combinations $\Delta\mathcal{A}_3 = \Delta\mathcal{U} - \Delta\mathcal{D}$ and $\Delta\mathcal{A}_8 = \Delta\mathcal{U} + \Delta\mathcal{D} - 2\Delta\mathcal{S}$, and the singlet $\Delta\Sigma = \Delta\mathcal{U} + \Delta\mathcal{D} + \Delta\mathcal{S}$. Had we data at only one Q^2, the two structure functions $g_1^{p,n}$ could not provide enough information to determine the full set $\Delta\mathcal{A}_3$, $\Delta\mathcal{A}_8$, $\Delta\Sigma$ at this Q^2. When information at different Q^2 is available, one can combine the data with knowledge about QCD evolution. In particular, each non-singlet quantity evolves separately from all other quantities, whereas $\Delta\Sigma$ mixes with the polarized gluon density $\Delta g(x, Q^2)$ in terms of a matrix evolution equation (10, 173). Thanks to this property under evolution, $g_1^{p,n}(x, Q^2)$ give in principle access to all four quantities, $\Delta\mathcal{A}_3$, $\Delta\mathcal{A}_8$, $\Delta\Sigma$, and Δg (174, 175). We note that, when performing fits to data in practice, one usually also includes constraints on the "first moments" (Bjorken-x integrals) of $\Delta\mathcal{A}_{3,8}$ derived from the β-decays of the baryon octet, the constraint on $\Delta\mathcal{A}_3$ being essentially the Bjorken sum rule (176). In this way, one is also able to better determine the first moment of $\Delta\Sigma$, which corresponds to the fraction of the proton spin carried by quarks and antiquarks.

Information on $\Delta\mathcal{A}_3$, $\Delta\mathcal{A}_8$, $\Delta\Sigma$, and Δg is equivalent in a "three-flavor world" to information on $\Delta\mathcal{U}$, $\Delta\mathcal{D}$, $\Delta\mathcal{S}$, and Δg—this is what DIS data can provide in

principle. We emphasize again that inclusive DIS cannot give information on the quark and antiquark densities separately; it always determines only the $\Delta\mathcal{Q}$. To distinguish quarks from antiquarks, let alone to achieve a full flavor separation of the polarized sea, one needs to defer to other processes (see Section 4).

We do not address in detail the question of how well the present data, within their accuracies, do indeed constrain the quantities $\Delta\mathcal{A}_3$, $\Delta\mathcal{A}_8$, $\Delta\Sigma$, and Δg. For this we refer the reader to the growing number of phenomenological analyses of the polarized DIS data (64, 44, 174, 79, 177, 175). However, to give a very rough picture of the situation, we state that (*a*) $\Delta\mathcal{A}_3(x, Q^2)$ and $\Delta\Sigma(x, Q^2)$ are relatively well known in the kinematic regions where data exist; (*b*) the Bjorken sum rule (176) is confirmed by the data; (*c*) the first moment of $\Delta\Sigma$, and thus the quark-plus-antiquark spin contribution to the proton spin, is of the order of 25% or less (known as "spin surprise"); and (*d*) $\Delta\mathcal{A}_8(x, Q^2)$ and the spin gluon density $\Delta g(x, Q^2)$ are constrained very little by the data so far. Note that this finding for $\Delta\mathcal{A}_8$ implies also that the polarized strange density is still unknown to a large extent. The present situation concerning Δg is represented by Figure 22, which compares the polarized gluon densities of several recent NLO sets of spin-dependent parton distributions (64, 44, 79), all consistent with current DIS data. The wide range of possible gluon polarization expressed by the figure does not come as a surprise. For DIS, the gluon is only determined through the scaling violations of the structure functions $g_1^{p,n}$; however, so far only fixed-target polarized

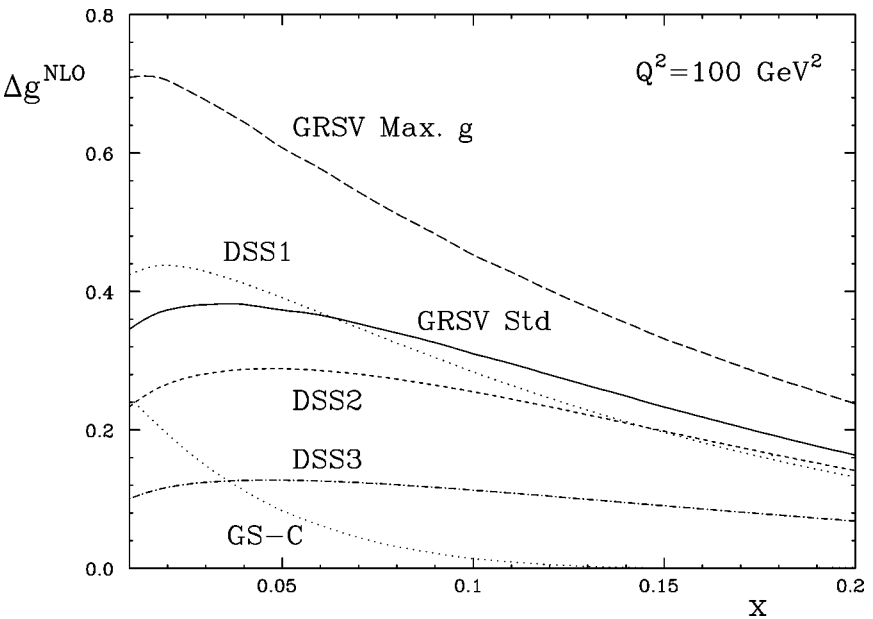

Figure 22 The polarized gluon densities as given by six different NLO parameterizations (64, 44, 79), at the scale $Q = 10$ GeV.

DIS experiments have been carried out, which have a limited lever arm in Q^2. The measurement of Δg remains one of the most interesting challenges for future high-energy experiments with polarized nucleons.

Visit the Annual Reviews home page at www.AnnualReviews.org

LITERATURE CITED

1. Ashman J, et al [European Muon Collaboration (EMC)]. *Phys. Lett.* B206:364 (1988); *Nucl. Phys.* B328:1 (1989); Adeva B, et al [Spin Muon Collaboration (SMC)]. *Phys. Rev. D* 58:112001 (1998); Anthony PL, et al (E142 Collaboration). *Phys. Rev. D* 54:6620 (1996); Abe K, et al (E143 Collaboration). *Phys. Rev. D* 58:112003 (1998); Abe K, et al (E154 Collaboration). *Phys. Rev. Lett.* 79:26 (1997); Anthony PL, et al (E155 Collaboration). *Phys. Lett.* B463:339 (1999); Ackerstaff K, et al (HERMES Collaboration). *Phys. Lett.* B404:383 (1997); Airapetian A, et al. *Phys. Lett.* B442:484 (1998); for review, see Hughes E, Voss R. *Annu. Rev. Nucl. Part. Sci.* 49:303 (1999)
2. Anselmino M, Efremov A, Leader E. *Phys. Rep.* 261:1 (1995); Erratum 281:399 (1997); Cheng HY. *Int. J. Mod. Phys.* A11:5109 (1996); *Chin. J. Phys.* 38:753 (2000); Lampe B, Reya E. *Phys. Rep.* 332:1 (2000); Bass SD. *Eur. Phys. J.* A5:17 (1999)
3. Collins J, Heppelmann SF, Robinett RW, eds. *Polarized Collider Workshop, AIP Conf. Proc.* 223 (1991)
4. Bunce G, et al. *Part. World* 3:1 (1992)
5. Derbenev YaS, Kondratenko AM. *Sov. Phys. JETP* 37:968 (1973); Derbenev YaS, et al. *Part. Acc.* 8:115 (1978)
6. Alekseev I, et al. *Design Manual Polarized Proton Collider at RHIC*, T Roser, spokesman (1998)
7. Lerach A, et al. C-AD/AP Note 10 (2000)
8. Libby SB, Sterman G. *Phys. Rev. D* 18:3252 (1978); Ellis RK, et al. *Phys. Lett.* 78B:281 (1978); *Nucl. Phys.* B152:285 (1979); Amati D, Petronzio R, Veneziano G. *Nucl. Phys.* B140:54 (1980); *Nucl. Phys.* B146:29 (1978); Curci G, Furmanski W, Petronzio R. *Nucl. Phys.* B175:27 (1980); Collins JC, Soper DE, Sterman G. *Phys. Lett.* B134:263 (1984); *Nucl. Phys.* B261:104 (1985)
9. Collins JC. *Nucl. Phys.* B394:169 (1993)
10. Altarelli G, Parisi G. *Nucl. Phys.* B126:298 (1977); Dokshitser YuL. *Sov. Phys. JETP* 46:641 (1977); Lipatov LN. *Sov. J. Nucl. Phys.* 20:95 (1975); Gribov VN, Lipatov LN. *Sov. J. Nucl. Phys.* 15:438 (1972)
11. Jaffe RL, Ji X. *Phys. Rev. Lett.* 67:552 (1991); *Nucl. Phys.* B375:527 (1992)
12. Ji X. *Phys. Rev. D* 49:114 (1994)
13. Ratcliffe PG. *Phys. Lett.* B192:180 (1987); Ramsey GP, Qiu J, Richards D, Sivers D. *Phys. Rev. D* 39:361 (1989); Jaffe RL. *Phys. Lett.* B365:359 (1996); Ji X, Tang J, Hoodbhoy P. *Phys. Rev. Lett.* 76:740 (1996); Ji X. *Phys. Rev. Lett.* 78:610 (1997); *Phys. Rev. D* 55:7114 (1997); Bashinsky SV, Jaffe RL. *Nucl. Phys.* B536:303 (1998); Hoodbhoy P, Ji X, Lu W. *Phys. Rev. D* 59:014013 (1999); Hägler P, Schäfer A. *Phys. Lett.* B430:179 (1998); Harindranath A, Kundu R. *Phys. Rev. D* 59:116013 (1999)
14. Craigie NS, Hidaka K, Jacob M, Renard FM. *Phys. Rep.* 99:69 (1983); Bourrely C, Soffer J, Leader E. *Phys. Rep.* 59:95 (1980)
15. Ralston JP, Soper DE. *Nucl. Phys.* B152:109 (1979); Cortes JL, Pire B, Ralston JP. *Z. Phys. C* 55:409 (1992)
16. Ji X. *Phys. Lett.* B289:137 (1992)
17. Artru X, Mekhfi M. *Z. Phys. C* 45:669. (1990)
18. Kane GL, Pumplin J, Repko W. *Phys. Rev. Lett.* 41:1689 (1978)
19. Sivers D. *Phys. Rev. D* 41:83 (1990); *Phys. Rev. D* 43:261 (1991)

20. Jaffe RL, Saito N. *Phys. Lett.* B382:165 (1996)
21. Goldhaber M, Grodzins L, Sunyar AW. *Phys. Rev.* 109:1015 (1958)
22. Schwinger J. *Phys. Rev.* 73:407 (1948)
23. Buttimore NH, Gotsman E, Leader E. *Phys. Rev. D* 18:694 (1978)
24. Kopeliovich BZ, Zakharov BG. *Phys. Lett.* B226:156 (1989)
25. Trueman TL. *Proc. Spin 96, Amsterdam, Sep. 1996*, ed. CW de Jager, et al, p. 833. hep-ph/9610429 (1996); RHIC/DET Note 18. hep-ph/9610316 (1996)
26. Bourrely C, Soffer J. *Proc. Spin 96, Amsterdam, Sep. 1996*, ed. CW de Jager, et al, p. 825. hep-ph/9610429 (1996)
27. Morrison DP, et al (PHENIX Collaboration). *Nucl. Phys.* A638:565c (1998)
28. Harris JW, et al (STAR Collaboration). *Nucl. Phys.* A566:277c (1994)
29. Draper PA (PP2PP Collaboration). Presented at 11th Int. Symp. High-Energy Spin Phys. and 8th Int. Symp. Polarization Phenomena in Nucl. Phys. (SPIN 94), Bloomington, Indiana, Sep. 1994
30. Videbaek F, et al (BRAHMS Collaboration). *Nucl. Phys.* A566:299c (1994)
31. Baker M, et al (PHOBOS Collaboration). QM95; Trzupek A, et al (PHOBOS Collaboration). *Acta Phys. Polon.* B27:3103c (1996)
32. Airapetian A, et al (HERMES Collaboration). *Phys. Rev. Lett.* 84:2584 (2000)
33. Mallot GK. hep-ex/9611016 (1996)
34. De Roeck A, et al. *Eur. Phys. J. C* 6:121 (1999)
35. Vogelsang W, Whalley MR. *J. Phys.* G23 (Suppl. 7A):A1 (1997)
36. Mobed N, Papavasiliou C, Svec M. *Phys. Rev. D* 26:3284 1982; Berger EL, Qiu J. *Phys. Rev. D* 40:778 (1989)
37. Gupta S, Indumathi D, Murthy MVN. *Z. Phys. C* 42:493 (1989); Erratum C44:356 (1989); Mathews P, Ramachandran R. *Z. Phys. C* 53:305 (1992)
38. Cheng HY, Lai SN. *Phys. Rev. D* 41:91 (1990)
39. Bourrely C, Guillet JPh, Soffer J. *Nucl. Phys.* B361:72 (1991); Chiappetta P, Colangelo P, Guillet JPh, Nardulli G. *Z. Phys. C* 59:629 (1993)
40. Bland LC. Presented at Workshop Phys. Electron Polarized Ion Collider—EPIC '99, Bloomington, Indiana, Apr. 1999, hep-ex/9907058 (1999)
41. Martin AD, Roberts RG, Stirling WJ, Thorne RS. *Eur. Phys. J. C* 4:463 (1998)
42. Lai HL, et al (CTEQ Collaboration). *Eur. Phys. J. C* 12:375 (2000)
43. Glück M, Reya E, Vogt A. *Eur. Phys. J. C* 5:461 (1998)
44. Gehrmann T, Stirling WJ. *Phys. Rev. D* 53:6100 (1996)
45. Buskulic D, et al (ALEPH Collaboration). *Z. Phys. C* 69:365 (1996); Ackerstaff K, et al (OPAL Collaboration). *Eur. Phys. J. C* 2:39 1998
46. Aurenche P, et al. *Nucl. Phys.* B399:34 (1993)
47. Glück M, Gordon LE, Reya E, Vogelsang W. *Phys. Rev. Lett.* 73:388 (1994)
48. Vogelsang W, Vogt A. *Nucl. Phys.* B453:334 (1995)
49. Aurenche P, et al. *Eur. Phys. J. C* 9:107 (1999)
50. Glück M, Reya E, Vogt A. *Phys. Rev. D* 48:116 (1993); Erratum *Phys. Rev. D* 51:1427 (1995)
51. Bourhis L, Fontannaz M, Guillet JPh. *Eur. Phys. J. C* 2:529 (1998)
52. Berger EL, Qiu J. *Phys. Rev. D* 44:2002 (1991)
53. Frixione S. *Phys. Lett.* B429:369 (1998)
54. Contogouris AP, Kamal B, Merebashvili Z, Tkachov FV. *Phys. Lett.* B304:329 (1993); *Phys. Rev. D* 48:4092 (1993)
55. Gordon LE, Vogelsang W. *Phys. Rev. D* 48:3136 (1993)
56. Contogouris AP, Merebashvili Z. *Phys. Rev. D* 55:2718 (1997)
57. Gordon LE, Vogelsang W. *Phys. Rev. D* 49:170 (1994)
58. Gordon LE. *Nucl. Phys.* B501:197 (1997);

Gordon LE, Ramsey GP. *Phys. Rev. D* 59:074018 (1999)
59. Chang S, Coriano C, Gordon LE. *Phys. Rev. D* 58:074002 (1998)
60. Frixione S, Vogelsang W. *Nucl. Phys.* B568:60 (2000)
61. Goto Y. Presented at Int. Workshop Deep Inelastic Scattering and QCD (DIS 99), 7th, Zeuthen, Ger., Apr. 1999; Goto Y, Hayashi N, Saito N. *Background Study for Prompt Photon Production at* PHENIX (internal RIKEN rep.) (1998)
62. Güllenstern S, Gornicki P, Mankiewicz L, Schäfer A. *Phys. Rev. D* 51:3305 (1995); Martin O, Schäfer A. hep-ph/0005320; Skoro GP, Zupan M, Tokarev MV. *Nuovo Cim.* A112:809 (1999)
63. Martin O. PhD thesis. Univ. Regensburg (1999)
64. Glück M, Reya E, Stratmann M, Vogelsang W. *Phys. Rev. D* 53:4775 (1996)
65. Abe F, et al (CDF Collaboration). *Phys. Rev. Lett.* 73:2662 (1994); Erratum 74: 1891 (1995); Kuhlmann S (CDF Collaboration). FERMILAB-CONF-99-165-E; Apanasevich L, et al (E706 Collaboration). *Phys. Rev. Lett.* 81:2642 1998; Ballocchi G, et al (UA6 Collaboration). *Phys. Lett.* B436:222 (1998)
66. Huston J, et al. *Phys. Rev. D* 51:6139 (1995); Baer H, Hall Reno M. *Phys. Rev. D* 54:2017 (1996); Apanasevich L, et al. *Phys. Rev. D* 59:074007 (1999); Begel M. PhD thesis. Rochester Univ., Rochester, NY (1999)
67. Kimber MA, Martin AD, Ryskin MG. *Eur. Phys. J.* C12:655 (2000)
68. Lai HL, Li H. *Phys. Rev. D* 58:114020 (1998)
69. Laenen E, Oderda G, Sterman G. *Phys. Lett.* B438:173 (1998); Catani S, Mangano ML, Nason P. *JHEP* 9807:024 (1998)
70. Catani S, et al. *JHEP* 9903:025 (1999)
71. Laenen E, Sterman G, Vogelsang W. *Phys. Rev. Lett.* 84:4296 (2000)
72. Leader E, Sridhar K. *Phys. Lett.* B311:324 (1993); *Nucl. Phys.* B419:3 (1994)
73. Berger EL, Gordon LE, Klasen M. *Phys. Rev.* D62:014014 (2000)
74. Babcock J, Monsay E, Sivers D. *Phys. Rev. Lett.* 40:1161 (1978); *Phys. Rev. D* 19:1483 (1979); Cheng HY, Hwang SR, Lai SN. *Phys. Rev. D* 42:2243 (1990); Ramsey GP, Sivers D. *Phys. Rev. D* 43:2861 (1991); Chiappetta P, Nardulli G. *Z. Phys. C* 51:435 (1991); Doncheski MA, Robinett RW, Weinkauf L. *Phys. Rev. D* 44:2717 (1991); Indumathi D, Murthy MVN, Ravindran V. *Z. Phys. C* 56:427 (1992); Soffer J, Virey JM. *Nucl. Phys.* B509:297 (1998)
75. de Florian D, Frixione S, Signer A, Vogelsang W. *Nucl. Phys.* B539:455 (1999)
76. Frixione S. *Nucl. Phys.* B507:295 (1997)
77. Frixione S, Kunszt Z, Signer A. *Nucl. Phys.* B467:399 (1996)
78. Babukhadia L. Presented at 35th Rencontres de Moriond: QCD and High Energy Hadronic Interactions, Les Arcs, France, March 2000. hep-ex/0005026 (2000)
79. de Florian D, Sampayo OA, Sassot R. *Phys. Rev. D* 57:5803 (1998)
80. Ellis S, Soper DE. *Phys. Rev. D* 48:3160 (1993)
81. Contogouris AP, Papadopoulos S, Kamal B. *Phys. Lett.* B246:523 (1990)
82. Karliner M, Robinett RW. *Phys. Lett.* B324:209 (1994)
83. Kamal B, Merebashvili Z, Contogouris AP. *Phys. Rev. D* 51:4808 (1995); (E) *Phys. Rev. D* 55:3229 (1997)
84. Bojak I, Stratmann M. *Phys. Lett.* B433:411 (1998); *Nucl. Phys.* B540:345 (1999)
85. Merebashvili ZV, Contogouris AP, Grispos G. hep-ph/9911506 (1999)
86. Bojak I, Stratmann M. Presented at RIKEN-BNL workshops "Predictions and Uncertainties for RHIC Spin Phys." and "Event Generator for RHIC Spin Phys. III," Brookhaven Natl. Lab., Upton, NY, March 2000; Bojak I. Doctoral thesis. Univ. Dortmund, Dortmund, Ger. hep-ph/0005120 (2000)

87. Frixione S, Mangano ML, Nason P, Ridolfi G. In *Heavy Flavours II*, ed. AJ Buras, M Lindner, p. 609. Singapore: World Sci. (1997)
88. Chang CH. *Nucl. Phys.* B172:425 (1980); Berger EL, Jones D. *Phys. Rev. D* 23:1521 (1981); Baier R, Rückl R. *Phys. Lett.* 102B:364 (1981)
89. Abe F, et al (CDF Collaboration). *Phys. Rev. Lett.* 69:3704 (1992); *Phys. Rev. Lett.* 71:2537 (1993)
90. Bodwin GT, Braaten E, Lepage P. *Phys. Rev. D* 51:1125 (1995)
91. Hidaka K. *Proc. Int. Symp. High-Energy Phys. with Polarized Beams and Polarized Targets, Lausanne, Switz.*, ed. C Joseph, J Soffer, p. 77 (1980)
92. Doncheski MA, Robinett RW. *Phys. Lett.* B248:188 (1990); *Z. Phys. C* 63:611 (1994); Robinett RW. *Phys. Rev. D* 43:113 (1991); Morii T, Tanaka S, Yamanishi T. *Phys. Lett.* B372:165 (1996); Braaten E, Chen YQ. *Phys. Rev. D* 54:3216 (1996)
93. Teryaev O, Tkabladze A. *Phys. Rev. D* 56:7331 (1997); Gupta S, Mathews P. *Phys. Rev. D* 55:7144 (1997)
94. Jaffe RL, Kharzeev D. *Phys. Lett.* 455:306 (1999); Cortes JL, Pire B. *Phys. Rev. D* 38:3586 (1988); Batunin AV, Slabospitsky SR. *Phys. Lett.* B188:269 (1987)
95. Lipkin HJ. *Phys. Lett.* B256:284 (1991); *Phys. Lett.* B337:157 (1994); Lichtenstedt J, Lipkin HJ. *Phys. Lett.* B353:119 (1995)
96. Amaudruz P, et al (NMC). *Phys. Rev. Lett.* 66: 2712 (1991); Arneodo M, et al (EMC). *Phys. Rev. D* 50:R1 (1994)
97. Baldit A, et al (NA51 Collaboration). *Phys. Lett.* 332:244 (1994); Hawker EA, et al (E866 Collaboration). *Phys. Rev. Lett.* 80:3715 (1998)
98. Ackerstaff K, et al (HERMES Collaboration). *Phys. Rev. Lett.* 25:5519 (1998)
99. Adeva B, et al (SMC). *Phys. Lett.* B420:180 (1998); Ackerstaff K, et al (HERMES Collaboration). *Phys. Lett.* B464:123 (1999)
100. Bourrely C, Soffer J. *Phys. Lett.* B314:132 (1993); *Nucl. Phys.* B423:329 (1994); Chiappetta P, Soffer J. *Phys. Lett.* B152:126 (1985)
101. Bourrely C, Soffer J. *Nucl. Phys.* B445341 (1995)
102. Kamal B. *Phys. Rev. D* 57:6663 (1998)
103. Gehrmann T. *Nucl. Phys.* B534:21 (1998)
104. Richter-Was E, Szwed J. *Phys. Rev. D* 31:633 (1985)
105. Mathews P, Ravindran V. *Mod. Phys. Lett.* A7:2695 (1992)
106. Altarelli G, Ellis RK, Martinelli G. *Nucl. Phys.* B157:461 (1979); Ratcliffe PG. *Nucl. Phys.* B223:45 (1983); Weber A. *Nucl. Phys.* B382:63 (1992)
107. Bland LC. Presented at Circum-Pan-Pacific RIKEN Symp. High Energy Spin Phys. (Pacific Spin 99), Wako, Jpn., Nov. 1999. hep-ex/0002061 (2000)
108. Sjostrand T. *Comput. Phys. Commun.* 82:74 (1994)
109. Balazs C, Yuan C.-P. *Phys. Rev. D* 56:5558 (1997)
110. Abe F, et al (CDF Collaboration). *Phys. Rev. Lett.* 74:850 (1995); *Phys. Rev. Lett.* 81:5754 (1998)
111. Gottfried K. *Phys. Rev. Lett.* 18:1174 (1967)
112. CTEQ Collaboration, Lai HL, et al. *Phys. Rev. D* 55:1280 (1997)
113. Martin AD, Roberts RG, Stirling WJ, Thorne RS. *Eur. Phys. J.* C14:133 (2000)
114. Bunce G, et al. *Phys. Rev. Lett.* 36:1113 (1976); Heller K, et al. *Phys. Lett.* B68:480 (1977); Gourlay SA, et al. *Phys. Rev. Lett.* 56:2244 (1986); Adams DL, et al. *Phys. Lett.* B261:201 (1991); *Phys. Lett.* B264:462 (1991); Bravar A, et al. *Phys. Rev. Lett.* 77:2626 (1996); Heller K. *Proc. Spin 96, Amsterdam, Sep. 1996*, ed. CW de Jager, et al, p. 23; Krueger K, et al. *Phys. Lett.* B459:412 (1999)
115. Goldstein GR, Jaffe RL, Ji X. *Phys. Rev. D* 52:5006 (1995)
116. Jaffe RL. *Proc. Workshop Deep Inelastic Scattering Off Polarized Targets,*

Phys. with Polarized Protons at HERA, DESY Zeuthen, Sept. 1997, p. 167. hep-ph/9710465 (1997)
117. Soffer J. *Phys. Rev. Lett.* 74:1292 (1995); Sivers *D. Phys. Rev. D* 51:4880 (1995)
118. Barone V. *Phys. Lett.* B409:499 (1997)
119. Vogelsang W. *Phys. Rev. D* 57:1886 (1998)
120. Bourrely C, Soffer J, Teryaev OV. *Phys. Lett.* B420:375 (1998)
121. Martin O, Schäfer A, Stratmann M, Vogelsang W. *Phys. Rev. D* 57:3084 (1998); *Phys. Rev. D* 60:117502 (1999)
122. Hayashigaki A, Kanazawa Y, Koike Y. *Phys. Rev. D* 56:7350 (1997); Kumano S, Miyama M. *Phys. Rev. D* 56:2504 (1997)
123. Ji X. *Phys. Lett.* B284:137 (1992)
124. Vogelsang W, Weber A. *Phys. Rev. D* 48:2073 (1993)
125. Contogouris AP, Kamal B, Merebashvili Z. *Phys. Lett.* B337:169 (1994)
126. Barone V, Calarco T, Drago A. *Phys. Rev. D* 56:527 (1997)
127. Miyama M. *Nucl. Phys. Proc. Suppl.* 79:620 (1999)
128. Scopetta S, Vento V. *Phys. Lett.* B424:25 (1998); *Phys. Lett.* B478:121 (2000)
129. Contogouris AP, Veropoulos G, Merebashvili Z, Grispos G. *Phys. Lett.* B442:374 (1998); *Nucl. Phys. Proc. Suppl.* 74:72 (1999)
130. Kamal B, Contogouris AP, Merebashvili Z. *Phys. Lett.* B376:290 (1996)
131. Collins JC, Heppelmann SF, Ladinsky GA. *Nucl. Phys.* B420:565 (1994); Collins JC, Ladinsky GA. hep-ph/9411444 (1994)
132. Jaffe RL, Jin X, Tang J. *Phys. Rev. Lett.* 80:1166 (1998); *Phys. Rev. D* 57:5920 (1998)
133. Collins JC. *Nucl. Phys.* B396:161 (1993)
134. Grosse-Perdekamp M (PHENIX), Ogawa A (STAR). Presented at RIKEN-BNL workshops "Predictions and Uncertainties for RHIC Spin Phys." and "Event Generator for RHIC Spin Phys. III," Brookhaven Natl. Lab. Upton, NY, March 2000
135. Efremov AV, Teryaev OV. *Phys. Lett.* 150B:383 (1985); *Sov. J. Nucl. Phys.* 36:140 (1982); 39:962 (1984)
136. Qiu J, Sterman G. *Phys. Rev. Lett.* 67:2264 (1991); *Nucl. Phys.* B378:51 (1992)
137. Adams DL, et al. *Phys. Lett.* B264:462 (1991)
138. Qiu J, Sterman G. *Phys. Rev. D* 59:014004 (1999)
139. Kanazawa Y, Koike Y. *Phys. Lett.* B478:121 (2000)
140. Boer D. *Phys. Rev. D* 60:014012 (1999)
141. Anselmino M, Boglione M, Murgia F. *Phys. Lett.* B362:164 (1995); *Phys. Rev. D* 60:054027 (1999); Anselmino M, Murgia F. *Phys. Lett.* B442:470 (1998)
142. Sivers D. Proc. Deep Inelastic Scattering off Polarized Targets: Theory Meets Experiment, Zeuthen 1997, ed. J Blümlein, et al, p. 383. DESY 97-200 (1997)
143. Boglione M, Leader E. *Phys. Rev. D* 61:114001 (2000)
144. Buskulic D, et al (ALEPH Collaboration). *Phys. Lett.* B374:319 (1996); paper LP279 submitted to Int. Symp. Lepton Photon Interact., XVIII, Hamburg, Ger., 1997; DELPHI Collaboration. DELPHI 95-86 PHYS 521, paper submitted to EPS-HEP 95 conf., Brussels, Belg., 1995; Ackerstaff K, et al (OPAL Collaboration). *Eur. Phys. J. C* 2:49 (1998)
145. de Florian D, Stratmann M, Vogelsang W. *Phys. Rev. D* 57:5811 (1998)
146. Ma BQ, Schmidt I, Yang JJ. *Phys. Rev. D* 61:034017 (2000)
147. de Florian D, Stratmann M, Vogelsang W. *Phys. Rev. Lett.* 81:530 (1998)
148. Boros C, Londergan JT, Thomas AW. *Phys. Rev.* D62:014021 (2000)
149. Burkardt M, Jaffe RL. *Phys. Rev. Lett.* 70:2537 (1993); Jaffe RL. *Phys. Rev. D* 54:6581 (1996)
150. de Florian D, Soffer J, Stratmann M, Vogelsang W. *Phys. Lett.* B439:176 (1998)
151. Bourrely C, et al. *Phys. Rep.* 177:319

(1989); Taxil P. *Polarized Collider Workshop, AIP Conf. Proc. 223,* ed. J Collins, SF Heppelmann, RW Robinett, p. 169 (1991); Tannenbaum MJ, *Polarized Collider Workshop, AIP Conf. Proc. 223,* ed. J Collins, SF Heppelmann, RW Robinett, p. 201
152. Taxil P, Virey JM. *Phys. Lett.* B364:181 (1995); *Phys. Rev. D* 55:4480 (1997)
153. Abott B, et al (DØ Collaboration). *Phys. Rev. Lett.* 82:2457 (1999)
154. Taxil P, Virey JM. *Phys. Lett.* B383:355 (1996); *Phys. Lett.* B441:376 (1998)
155. Lykken JD. *Snowmass 1996*, ed. DG Cassel, L Trindle Gennari, RH Siemann, p. 891; Lopez JL, Nanopoulos DV. *Phys. Rev. D* 55:397 (1997); Babu KS, Kolda C, March-Russell J. *Phys. Rev. D* 54:4635 (1996); Faraggi AE, Masip M. *Phys. Lett.* B388:524 (1996)
156. Agashe K, Graesser M, Hinchliffe I, Suzuki M. *Phys. Lett.* B385:218 (1996); Georgi H, Glashow SL. *Phys. Lett.* B387:341 (1996)
157. Cvetič M, et al. *Phys. Rev. D* 56:2861 (1997)
158. Rykov VL. hep-ex/9908050 (1999)
159. Kovalenko S, Schmidt I, Soffer J. hep-ph/9912529 (1999)
160. Boer D. hep-ph/0004217 (2000)
161. Akchurin N, et al. *Phys. Lett.* B229:299 (1989); *Phys. Rev. D* 48:3026 (1993)
162. Particle Data Group. *Eur. Phys. J. C* 3:206 (1998)
163. Cheng H, Wu TT. *Phys. Rev. Lett.* 24:1456 (1970)
164. Bourrely C, Soffer J, Wu TT. *Nucl. Phys.* B247:15 (1984)
165. Drees M, Kim CS, Kim SK, eds. *Proc. APCTP Workshop: Pacific Particle Phys. Phenomenol., Seoul, Korea, 1997.* Singapore: World Sci. (1998)
166. Buttimore N, et al. *Phys. Rev. D* 59: 114010 (1999)
167. Bourrely C, Soffer J, Wray D. *Nucl. Phys.* B91:33 (1975)
168. Ryskin MG. *Yad. Fiz.* 46:611 (1987); *Sov. J. Phys.* 46:337 (1987)
169. Zakharov BG. *Sov. J. Nucl. Phys.* 49:860 (1989)
170. Collins PDB, Squires EJ. *Springer Tracts in Modern Physics* 44. Berlin: Springer-Verlag (1968); Forshaw JR, Ross DA. *Lecture Notes in Physics* 9. Cambridge, UK: Cambridge Univ. Press (1997)
171. Gauron P, Leader E, Nicolescu B. *Phys. Rev. Lett.* 54:2656 (1985); Donnachie A, Landshoff PV. *Nucl. Phys.* B267:690 (1986)
172. Leader E, Trueman TL. *Phys. Rev. D* 61: 077504 (2000)
173. Ahmed MA, Ross GG. *Nucl. Phys.* B111:441 (1976)
174. Altarelli G, Ball RD, Fortev S, Ridolfi G. *Nucl. Phys.* B496:337 (1997)
175. Leader E, Sidorov AV, Stamenov DB. *Phys. Rev. D* 58:114028 (1998)
176. Bjorken JD. *Phys. Rev.* 148:1467 (1966)
177. Adams D, et al (SMC). *Phys. Rev. D* 56:5330 (1997); Adeva B, et al (SMC). *Phys. Rev. D* 58:112002 (1998)